NACA

RESEARCH MEMORANDUM

PERFORMANCE OF A BLUNT-LIP SIDE INLET WITH RAMP BLEED,

BYPASS, AND A LONG CONSTANT-AREA DUCT AHEAD OF

THE ENGINE: MACH NUMBERS 0.66 AND 1.5 TO 2.1

By John L. Allen

Lewis Flight Propulsion Laboratory
Cleveland, Ohio

Declassified February 8, 1963

NATIONAL ADVISORY COMMITTEE
FOR AERONAUTICS
WASHINGTON

December 28, 1956

4186

CH-1

NATIONAL ADVISORY COMMITTEE FOR AERONAUTICS

RESEARCH MEMORANDUM

PERFORMANCE OF A BLUNT-LIP SIDE INLET WITH RAMP BLEED, BYPASS,

AND A LONG CONSTANT-AREA DUCT AHEAD OF THE ENGINE:

MACH NUMBERS 0.66 AND 1.5 TO 2.1

By John L. Allen

SUMMARY

The performance of a side inlet having a fixed 12° two-dimensional compression surface was determined at Mach numbers of 0.66 and 1.5 to 2.1 for a range of angles of attack and yaw. The effects of several methods of compression-surface boundary-layer removal were investigated as well as a solid ramp.

At Mach numbers 2.0 and 1.7 shock-induced separation of the ramp boundary layer became progressively unsteady as mass-flow ratio was reduced and caused a corresponding increase in static-pressure fluctuations at the diffuser exit. Compression-surface bleed reduced and stabilized the shock-induced separation and thus extended the usable range of stable mass-flow ratio. Peak pressure recovery occurred just before minimum stable flow.

Of the various types of boundary-layer bleed, external perforations gave the greatest gains in pressure recovery and stability. At Mach 2.0 peak pressure recovery was increased from 0.802 for the solid ramp to 0.89; and stability range, from about 0.10 to 0.285, in terms of mass-flow ratio from the critical value. Distribution and density of perforations were important factors. For the same bleed flow area, external slots were less effective than perforations. Although the stability range was generally smallest for internal bleed, the level of pressure recoveries within the stable region was higher than for external bleed.

A 5-diameter constant-area section followed by overexpansion and contraction between the diffuser exit and compressor inlet was very effective in reducing large values of total-pressure distortion for a total-pressure recovery loss of less than 4 percent. With throat bleed, distortion at the diffuser exit was appreciably reduced, and the long duct was less effective. A flush-type bypass near the compressor face tended to offset the total-pressure loss caused by the long duct by removing the boundary layer generated therein.

Excellent angle-of-attack characteristics were obtained with both the solid and perforated ramps.

INTRODUCTION

The performance of a side inlet for a proposed twin-engine supersonic interceptor has been determined in the NACA Lewis 8- by 6-foot supersonic tunnel. Features of the air induction system included: (1) a fixed-angle two-dimensional compression surface, (2) internal contraction that exceeded the starting limit, (3) a low-angle, rounded-lip cowl, (4) a long constant-area section followed by overdiffusion and rapid contraction between the diffuser exit and the compressor inlet, (5) a flush-type bypass ahead of the compressor inlet, and (6) provisions for ramp boundary-layer bleed.

Axial-force and pressure-recovery data were determined for a solid ramp, for various patterns of perforations and flush slot sizes on the external portion of the compression ramp, and for a lesser number of similar bleed devices in the region of the throat. The performance of the solid and most promising perforated ramps was evaluated for Mach numbers of 0.66 and 1.5 to 2.1, angles of attack from $-2\frac{1}{2}^{\circ}$ to $9\frac{1}{2}^{\circ}$, and angles of yaw from $2\frac{1}{2}^{\circ}$ windward to 6° leeward. The total-pressure loss and the change in total-pressure distortion between the diffuser exit and the engine face was determined. The effects of several sizes of the bypass slot on total-pressure recovery and distortion were also determined; however, it was not possible to obtain force data for the bypass condition.

SYMBOLS

A area, sq ft

A_c inlet capture area, 0.283 sq ft

A_{max} model frontal area, 1.138 sq ft

A_3 diffuser-exit area, station 3, 0.196 sq ft

A_4 compressor-inlet area, station 4, 0.1873 sq ft

$C_{\mathcal{F}}$ axial-force coefficient, $\dfrac{\mathcal{F}}{q_0 A_{max}}$

$F_{n,ej}$ engine net thrust with ejector nozzle

$F_{n,i,conv}$ engine ideal net thrust, 100 percent ram, convergent nozzle

$\mathcal{F}$ axial force

H total pressure

$\dfrac{\Delta H}{H_{av}}$ total-pressure distortion parameter, numerical difference between maximum and minimum rake total pressures divided by average total pressure, percent

h boundary-layer splitter height, 0.4 in.

M Mach number

m/m_0 mass-flow ratio, $\dfrac{\rho V A}{\rho_0 V_0 A_c}$

p static pressure

q dynamic pressure

V velocity

w weight flow, lb/sec

$\dfrac{w\sqrt{\theta}}{\delta A}$ corrected rate of weight flow of air per unit area, (lb/sec)/sq ft

x axial distance

α angle of attack, deg

δ ratio of total pressure to NACA standard sea-level static pressure of 2116 lb/sq ft

$\hat{\delta}$ fuselage boundary-layer thickness, in.

θ ratio of total temperature to NACA standard sea-level static temperature of 519° R

ρ mass density of air

ψ angle of yaw, deg

Subscripts:

B   bypass

b   bleed

R   ramp

th   throat

O   free stream

1   inlet survey station ahead of ramp

2   inlet survey station near throat $1\frac{1}{2}$ in. from cowl lip

3   diffuser exit

4   compressor inlet

Configuration designations:

A   external perforations

B   external slots

C   internal slots

D   internal perforations

S   various bypass slot sizes

V   vent installed on side of ramp

MODEL DETAILS, INSTRUMENTATION, AND METHODS OF CALCULATION

General Description of Model

Photographs of the 1/6-scale model are shown in figure 1, a schematic drawing is shown in figure 2, and the duct area variation is given in figure 3. The conical nose of the model (30° included angle), which was canted downward $3\frac{1}{2}°$ from the horizontal, was symmetrical back to the leading edge of the compression ramp; however, only one of the twin inlets was included on the model. The leading edges of the ramp and cowl were canted downward $7\frac{1}{4}°$ from the horizontal.

Main-Duct Air Induction System

A fixed 12° two-dimensional ramp with rather generous fillets fairing into the cowl lip and throat (fig. 1(c)) composed the inlet compression surface. These fillets resembled partial side-fairings. The low-angle rounded-lip cowl in conjunction with the ramp and throat fillets resulted in 22-percent internal contraction (A_{lip}/A_{throat}), which exceeds the starting limit for this ramp angle at Mach numbers below 2.5.

As shown on figure 3, the cross-sectional shape of the diffuser changed from practically oval at the throat (station 2) to circular at the diffuser exit (station 3). Between stations 2 and 3 the duct was turned in the vertical plane from the 7°15' downward cant to horizontal (fig. 2). The length of duct between the diffuser-exit and compressor-face stations (3 to 4) was about $7\frac{1}{3}$ diameters (station 3 diameter). A part of this length was composed of about 5 diameters of constant-area section within which the duct was turned 8°45' downward. Aft of this point duct flare resulted in overexpansion followed by contraction in the region of the accessory bullet. At the compressor face the duct was turned from 8°45' downward to 2°35' upward relative to the horizontal axis. Total angular turning of the entire duct in the vertical plane amounted to 27°20'. An annular flush-type bypass slot was slightly forward of the compressor-face survey station (fig. 2, detail C). In the airplane the bypass air is used as the secondary-air supply for an ejector exhaust nozzle.

Secondary-Air Induction Systems

Fuselage boundary-layer airscoop and diverter. - An open-nose type boundary-layer diverter separated the compression ramp from the fuselage by about 0.40 inch, which was approximately $1\frac{1}{3}$ thicknesses of the local boundary layer $(h/\hat{\delta} = 1.33)$ at zero angle of attack. The leading edges of this diverter were about 8.5 boundary-layer thicknesses aft of the ramp leading edge. Although the surfaces of the diverter were curved, the initial angle of each side was about 30°. Air captured by the diverter airscoop was ducted through the model and controlled by means of a plug (fig. 2).

Compression-surface bleed system. - A portion of the ramp was fitted with a removable section for installing various surface bleed devices. Detailed drawings of the external perforations are shown in figure 4(a), and drawings of the external or internal slots are presented in figure 4(b). Pertinent areas, area ratios, and configuration designations are

given in table I. For configurations A_1 to A_4 the thickness of the
perforated metal was about 1/32 inch. For A_4 the 1/8-inch holes were
3/8 to 1/4 inch deep. For A_5 to A_8 the metal thickness was 3/32
inch. The ramp bleed airflow was ducted through the model and controlled
by a plug. For some configurations additional bleed capacity was pro-
vided by opening the side of the ramp bleed chamber and installing a
wedge-shaped windshield. This is shown in figure 1(c) and is hereinafter
termed a vent (designated by V). For these configurations, only that
flow within the ducting system was measured.

Instrumentation

Pressure measurements. - In order to evaluate the effect of the
long duct between stations 3 and 4, duplicate tests were made for some
conditions with and without a total-pressure rake at station 3. The
removable rake at station 3 had six equally spaced radial segments com-
posed of 31 total-pressure tubes and six wall static-pressure orifices.
Twenty-four of the total-pressure tubes were arranged for area-weighting
with one tube at the duct center. Each rake segment had one total-
pressure tube near the duct wall at a radius of 0.985 that was used as
a limit for computing total-pressure distortions. The rake at station 4
had six equally spaced radial segments composed of 36 total-pressure
tubes and six static-pressure orifices on both the outer wall and the
accessory housing surfaces. Twenty-four total-pressure tubes were area-
weighted with extra tubes for distortion limits at radius ratios of 0.493
and 0.975. Hub-tip radius ratio was 0.468. For both rakes the tubes
used for distortion limits would be 1/2 inch from the surface of a full-
scale duct. An inlet throat total- and static-pressure survey was made
$1\frac{1}{2}$ inches aft of the cowl leading edge, or 1/4 inch aft of the geometric
throat. With this rake installed the minimum area was moved from $1\frac{1}{4}$ to
$2\frac{1}{2}$ inches aft of the lip and reduced about 2 percent.

Inlet flow angularity in both the pitch and yaw planes was deter-
mined at a station about 2 inches forward of the ramp leading edge by
means of four instrumented 12°-included-angle wedges. The wedges were
located 2 inches on either side of the duct centerline and 2.2 and 5.2
inches from the fuselage surface. Flow-deflection angles in the plane
normal to the fuselage did not differ appreciably, and hence all four
wedges were averaged to obtain the deflection at the centerline.

Base pressures were measured by five static-pressure orifices on
the rear bulkhead forward of the windshield that enclosed the mass-flow
plugs and tailpipe and also by five static tubes at the split of the
accessory bullet aft of the station 4 rake. A strain-gage dynamic-
pressure pickup was connected to a flush static-pressure orifice

installed slightly ahead of station 3. Each of the secondary-air ducts (diverter and ramp bleeds) had four wall static-pressure orifices and three area-weighted total-pressure tubes in a plane of survey that was preceded by about 20 diameters of constant-area length.

Force measurements. - Because of the asymmetric nature of the model (only one inlet) the strain-gage balance was used only for axial forces. That part of the model not falling within the minimum reflected-shock pattern had a constant-area cross section to minimize the effect on axial-force readings. The main-duct tailpipe within the windshield was connected to the balance, and no correction was made for the relatively minor effect of flow within the windshield (such as from the secondary-air ducts) on the outer surface of the pipe. Force data were not obtained with the bypass open.

Methods of Calculation

Pressure and mass flow. - As stated previously, all total-pressure recoveries were area-weighted. Total-pressure distortions were computed as the maximum minus the minimum divided by the average total pressure. All mass-flow ratios (based on main inlet capture area) were calculated by means of the ratio of average static to average total pressure at the respective survey planes. With the station 3 rake installed, the station 4 rake was used only for mass-flow calculations.

Axial-force coefficient. - The change in momentum in the axial direction between the free-stream and the exit measuring stations of all the airflow ducted through the model and base pressure forces were removed from the strain-gage balance force measurements. The axial-force coefficient is based on the maximum cross-sectional area of the force portion of the model. Main-duct exit momentum was computed by means of mass-flow continuity between station 4 and a static-pressure measuring station located aft of the rake and ahead of the centerbody split. Thus, the force on the rake was accounted for. With the vent installed on the ramp, the mass flow exiting from the vent was not measured, and hence the force due to this air is included in the axial-force coefficient.

PRESENTATION OF RESULTS

The data are presented in four groups:

(1) Inlet flow-field angularity (fig. 5)

(2) Performance of solid-ramp inlet at Mach numbers of 0.66, 1.5, 1.7, and 2.0 for angles of attack of $-2\frac{1}{2}^{\circ}$ to $9\frac{1}{2}^{\circ}$ and yaw angles

of $-2\frac{1}{2}^{O}$ windward to 6° leeward; effects of constant-area section and different bypass openings included (figs. 6 to 13)

(3) Performance of various ramp bleed methods at zero angle of attack (figs. 14 to 18)

(4) Detailed performance of a selected ramp bleed configuration at Mach numbers 0.66 and 1.5 to 2.1 at angles of attack from $-2\frac{1}{2}^{O}$ to $9\frac{1}{2}^{O}$ and angles of yaw from $-2\frac{1}{2}^{O}$ to 6°; incremental axial-force coefficients, stability limits, effective thrust ratio analyses included (figs. 19 to 23)

DISCUSSION

Inlet Flow-Field Survey

The inlet flow-field angularity, shown in figure 5, was generally independent of flight Mach number except for the effect of yaw angle at Mach 2.0. The variation of flow angle with angles of attack or yaw was nearly linear. At zero angle of attack the flow was nearly alined with the horizontal axis or downward $8\frac{1}{2}^{O}$ relative to the inlet centerline as a result of the $7\frac{1}{4}^{O}$ inlet cant. At an angle of attack of 6.7^{O} the inlet was approximately alined with the local flow. At zero yaw angle the flow deflection in the horizontal plane was outboard about 1^{O}, and for 6° leeward yaw was outboard about 4°.

The wedge survey data also indicated local Mach numbers and total pressures on the order of free-stream values. A fuselage boundary-layer thickness of about 0.30 inch or an h/δ of 1.33 at zero angle of attack was established by means of a total-pressure rake.

Performance with Solid Ramp

Qualitative description. - The progressive increase of ramp boundary-layer separation as mass-flow ratio was reduced is shown by the schlieren photographs of figure 6 and the throat total-pressure contours of figure 7.

Although the schlieren photograph (fig. 6(a)) near maximum mass-flow ratio at Mach number 2.0 $(m_4/m_0 = 0.773)$ indicates a lambda shock, no separation is evident in the corresponding throat total-pressure contour of figure 7(a). For subcritical mass-flow ratios, separation was

4186

CH-2

most severe at Mach number 2.0, evident at Mach 1.7, and insignificant at Mach 1.5. The reduction in pressure recovery accompanying increased separation at each Mach number is shown by the subcritical slope of the pressure-recovery - mass-flow curves in figure 8.

A distinguishing feature of the shock-induced separation of the ramp boundary layer was the instability or rapid fluctuation of the region of separated flow, which seemingly caused a corresponding static-pressure fluctuation at the diffuser exit. This occurred without the usual pulsing, buzz, or noticeable movement of the normal shock. At Mach number 2.0, for example, the static-pressure amplitude (near station 3) increased from about 8 percent of free-stream total pressure at a mass-flow ratio of 0.64 to about 15 percent at a mass-flow ratio of 0.45.

Peak total-pressure recovery and maximum mass-flow ratio. - Peak pressure recoveries were about 0.96, 0.905, and 0.802 at Mach numbers of 1.5, 1.7, and 2.0, respectively (fig. 8), for zero angle of attack. Theoretical choked-throat mass-flow ratios and total-pressure recoveries are indicated on figure 8 for a 12° ramp at free-stream conditions (oblique- plus normal-shock recoveries). The difference between theoretical and experimental peak pressure recoveries varied from 0.08 unit of pressure recovery (8 percent of free-stream total pressure) at Mach 2.0 to 0.01 unit at peak or 0.025 unit at critical at Mach 1.5. (Peak and critical pressure recoveries were about equal at Mach numbers 2.0 and 1.7 where ramp separation occurred subcritically.) At critical flow conditions the variation of this difference (0.08 to 0.025) with Mach number is primarily indicative of the effect of throat total-pressure contour (shape factor) on diffuser efficiency, inasmuch as the throat is choked for each flight Mach number. The theoretical maximum mass-flow ratios are in good agreement with the experimental data in spite of the inlet flow angularity, which has a second-order effect on ramp angle, and other minor assumptions (e.g., H_0, M_0 at ramp leading edge).

Effect of angles of attack or yaw. - The peak pressure recovery varied only 0.025 unit of pressure recovery between angles of attack of $-2\frac{1}{2}^{\circ}$ to $9\frac{1}{2}^{\circ}$ (fig. 8). The lowest peak recovery was consistently obtained at $-2\frac{1}{2}^{\circ}$ angle of attack, for which the local flow angle (fig. 5) is farthest from being alined with the inlet. Highest peak recovery, occurring between angles of attack of 5° and $9\frac{1}{2}^{\circ}$, agrees qualitatively with the flow-field angularity, which indicated alinement at 6.7°. The general insensitiveness to angle-of-attack effects is attributed to the standing bow shock, generous fillets, and round cowl lips.

Leeward yaw of 6° decreased peak recovery about 0.03 unit, whereas windward yaw of $2\frac{1}{2}^{\circ}$ increased recovery by about the same amount because

of favorable local Mach number reductions (fig. 9). The maximum mass-flow ratio was also affected by changes of local Mach number and total pressure due to yaw.

Effect of 5-diameter constant-area section followed by overdiffusion and rapid contraction. - The $7\frac{1}{3}$-diameter length of duct between the diffuser exit and the engine materially reduced total-pressure distortion (fig. 8). Most of this reduction is believed to be due to mixing actions. However, part of the distortion reduction may be fictitious, inasmuch as the outer tube at station 4 should be somewhat closer to the wall in order to follow a streamline from the outer tube at station 3. The total-pressure-recovery loss was between 0.03 to nearly 0 unit of recovery, depending on mass-flow ratio (fig. 10). For example, at zero angle of attack and Mach number 2.0, for critical flow (no ramp separation), a station 3 distortion of 21 percent was reduced to about 12.5 percent at station 4 for a total-pressure-recovery loss of 0.024. At a mass-flow ratio of 0.70, a 32-percent distortion was reduced to 10.7 percent for a loss of 0.017. Large values of distortion were found at station 3 when ramp separation was severe, such as shown for Mach numbers 2.0 and 1.7. At Mach number 1.5, however, where ramp separation did not occur to any large extent, the distortion at station 3 was lower and only slightly reduced at station 4. Leaving the station 3 rake installed apparently decreased the effectiveness of the constant-area section because of wakes from the rake and resulted in appreciably higher distortions at station 4, as shown by the solid symbols in figure 8. Comparative total-pressure contours at stations 3 and 4 are shown in figure 11. The change in position of the low-energy total-pressure region from alinement with the ramp at the throat to the top portion of the duct at station 3 suggests the existence of secondary flows due to duct turning. The low-energy region does not change location appreciably between stations 3 and 4 but spreads somewhat. (The net duct turning is small, and large area changes occur.) At a subsonic Mach number of 0.66, the flow is very symmetric.

Effect of bypass slot size. - Each of the three bypass positions, which progressively increased bypass flow area, resulted in peak pressure recoveries higher than that obtained without bypass (fig. 12). This increase, which was as much as 0.02 unit of pressure recovery, indicates removal of the boundary-layer growth that occurred between stations 3 and 4 and agrees well with the pressure-recovery losses shown in figure 10. The largest slot size, S_4, removed from 30 to 23 percent

of the flow entering the inlet. The decreases in distortion at peak recovery shown for the various bypass settings compared with the value at critical flow without bypass are related to the decrease in compressor-face Mach number or corrected weight flow per unit area, as discussed in reference 1. When compared at the equal values of corrected weight flow in the subcritical region, little difference is found. In general, the station 4 total-pressure contours shown in figure 13, together with those of figure 11 for the zero-bypass case, indicate gradual removal

of low-energy regions near the duct walls and spreading of the high-energy regions as the amount of bypassed flow is increased.

Performance of Ramp Bleed Devices

The performance obtained with external perforations (fig. 14) and internal perforation and internal or external slots (fig. 15) is summarized in the following table for Mach number 2.0 in terms of peak pressure recovery and stability range. Pertinent geometric information is given in table I and figure 4.

Configuration and flow area, sq in.	Peak pressure recovery	Stable mass-flow range, $\Delta m_4/m_0$	Bleed mass-flow ratio for maximum stability	Percent increase in	
				Pressure recovery	Stable range
Solid ramp	0.802	0.10		0	0
External perforations:					
A_1 0.52	0.826	0.10	0.003	3.1	0
A_2 1.16	.844	.13	.009	5.2	30
A_3 2.29	.852	.13	.02	6.2	30
A_4V 3.82	.876	.266	> .028	9.2	166
A_5 2.08	.864	.20	.021	7.7	100
A_6 3.47	.868	.198	.021	8.2	98
A_7V 4.69	.890	.278	> .03	11.0	178
A_8 2.74	.872	.248	.024	8.7	148
A_8V 2.74	.870	.285	> .023	8.5	185
External slots:					
B_1 0.64	0.825	0.11	0.006	2.9	10
B_2 1.60	.835	.145	.015	4.1	45
B_3 3.00	.852	.170	.02	6.2	70
Internal slots:					
C_3 3.00	0.857	0.146	0.04	6.9	46
C_4V 4.59	.850	.114	> .036	6.0	14
Internal perforation:					
D_1 0.52	0.831	0.154	0.009	3.6	54

All of the types of bleed increased peak pressure recovery and had stability ranges equal to or better than the solid ramp. The greatest increases were obtained with external perforations having the largest flow area and distribution of porosity. Total-pressure distortions were about equal to or less than those for the solid ramp.

External perforations. - Peak pressure recovery occurred just before the point of minimum stable mass-flow ratio and tended to correspond to maximum bleed mass-flow ratio (fig. 14). As the lambda shock pattern moved into the perforated region, bleed mass flow increased because of the shock pressure rise until the holes were choked or instability occurred. However, the importance of the distribution of flow area is demonstrated by the fact that increasing flow area did not in all cases offer proportional gains in recovery or stability. For example, nearly doubling the flow area without changing distribution of a pattern on the rear of the ramp, A_2 to A_3, changed pressure recovery only slightly and did not increase stability range in spite of increased bleed flow. Increasing porosity forward of that for A_3, such as A_4V (A_3 plus a concentration of larger size holes extending about 3/4 in. forward of A_3), offered marked increases in both recovery and stability. Reverting to a uniform distribution of perforations, A_5 (extending forward of that for A_4V), was less effective. Increasing the hole size of the forward portion of A_5 to make A_6 (similar to the change from A_3 to A_4V) was ineffective; and, since bleed flow increased only slightly, the shock pattern was probably not near enough to the enlarged holes to provide a choking pressure ratio. Enlarging the remainder of the holes in this pattern to form A_7V (which had the largest flow area) and installing the vent to ensure sufficient bleed-system capacity resulted in the largest pressure-recovery increase (11 percent) and a stability increase of 178 percent. The required bleed mass flow was somewhat greater than 6 percent of the flow that entered the inlet.

Inasmuch as extension of the perforated area towards the cowl lip (A_2 to A_3) or forward of A_4V (such as A_5) did not result in proportional improvements, configuration A_8V was devised in order to reduce perforated area and ducted bleed flow. As shown in the preceding table, this configuration had the largest stability range and the greatest increase in peak pressure recovery for this amount of flow area.

External slots. - The position on the ramp of the related series of external slots (B_1, B_2, B_3) did not change appreciably with slot size and corresponded approximately to the position of the perforated regions

4186

for A_1 or A_2. The increase in peak pressure recovery with bleed
slot area was linear. Stability range increased with slot area but not
linearly. The importance of flow-area distribution is again demonstrated
by the performance of B_3. This configuration had a slot area about
equal to the perforated area of A_8 but achieved only about 2/3 the
recovery and half the stability increases of A_8.

Internal slots and perforations. - Application of internal bleed in
the contracting region ahead of the throat (configurations C_3, C_4V, and
D_1) resulted in appreciably less stability and lower peak recoveries com-
pared with external perforations (fig. 15). The performance of C_3 and
B_3, which were of equal size, was comparable. Configuration C_4V, which
was slightly aft, larger, and had a different ramp approach surface
ahead of the slot, had about the same performance as C_3. The configu-
ration with internal perforations (D_1) was more effective with respect to
stability than those with a similar external pattern (A_1), but because
of the small area did not approach the performance of those having larger
flow area. All of the internal-bleed configurations had higher pressure
recoveries within the stable region than the external bleeds, inasmuch
as the normal shock was always ahead of the slot and bleed flow increased
rapidly as the shock moved forward.

Inlet instability with ramp bleed. - As previously discussed,
schlieren observation indicated a progressive increase in unstable sep-
aration of the ramp boundary layer as mass flow was reduced for the solid
ramp. In contrast, the bleed ramps had a reduced but stable separation
up to the point of minimum stable mass flow. Further mass-flow reduc-
tions resulted in unstable separation with brief periodic excursions into
what appeared to be separation that completely encompassed the inlet.
This was especially true for the perforated ramps having appreciable
stability, such as A_4V, A_7V, and A_8V. For these cases high-speed mo-
tion pictures qualitatively indicated that, because of the unsteady sep-
aration, the vortex sheet emanating from the junction of the terminal
shock and the oblique shock from the separated flow oscillated within
limits between the ramp surface and the cowl lip and occasionally inter-
sected the cowl lip. This intersection of the vortex sheet with the cowl
lip was followed by the complete separation of the ramp boundary layer
previously mentioned. These comments are illustrated in figure 16 for
configuration A_8V. Figure 16(a) for a mass-flow ratio of 0.536 just
before the minimum stable point shows the reduced separation (compared
with the solid-ramp schlieren for mass-flow ratio 0.587 at $M_0 = 2.0$

from fig. 6), and the steadiness of the separation is shown by the low value of 0.01 for the ratio of dynamic static-pressure amplitude to free-stream total pressure $\Delta p_3/H_0$. At a mass-flow ratio of 0.503 the schlieren photograph of figure 16(b) and clips from the high-speed motion pictures show some of the extreme positions of the separation for which the value of $\Delta p_3/H_0$ was in excess of 0.19.

Some effects of varying bleed flow. - For some of the configurations, slight gains in pressure recovery were found for reduced bleed mass-flow ratios, as shown in figure 17. The bleed mass-flow ratio plotted is only that ducted through the model, and hence configurations A_7V and A_8V still have vent bleed flow at $m_b/m_0 = 0$. As bleed mass-flow ratio approached zero, pressure recovery and stability tended to revert to solid-ramp values. Maximum stability range was in all cases attained with maximum bleed flow, such as shown in figure 17 for A_7V and A_8V with vent flow only and with vent plus maximum duct flow.

Effectiveness of long duct with ramp bleed. - Since throat bleed removed and controlled ramp separation, the distortion level at station 3 was appreciably less than for the solid ramp, as shown in figure 18 for configuration C_4V. At station 4, however, the distortion level was not significantly changed, indicating that the long duct length was not correspondingly effective when the initial distortion was lower. This is also shown by the fact that, when the distortion value did become high at station 3, such as when ramp bleed was not sufficient, the level at station 4 did not change correspondingly.

Performance of Configuration A_8V

The performance of configuration A_8V was determined in some detail with a bypass setting, S_1, chosen to approximate exhaust ejector pumping capacity for best net thrust gains. A much larger bypass setting, S_5, which might be used for engine idle or windmill situations, was also tested over limited conditions. The data are presented in figures 19, 20, and 21. Lines of turbojet corrected weight flow per unit area are superimposed on the plots for an altitude of 35,000 feet, and oil-cooler airflows are included.

Effects of Mach number and angles of attack or yaw. - The perforated ramp provided significant increases in pressure recovery and stability range from Mach numbers 1.5 to 2.0, as shown in figure 19. Increases were obtained even at Mach number 1.5 where ramp separation was not a problem. At Mach numbers 1.5 and 1.7, stability range was limited by available plug travel rather than by inlet performance.

For angles of attack between 0° and $9\frac{1}{2}^O$, only minor variations in pressure recovery were found at Mach number 2.0, and virtually no variation at Mach numbers 1.7 and 1.5. The reduction in pressure recovery due to a negative angle of attack of $-2\frac{1}{2}^O$ increased progressively with Mach number and, as for the solid ramp, was the most pronounced reduction due to angle of attack. The effect of yaw angle (fig. 20) was about the same as that obtained with the solid ramp with respect to pressure recovery and mass-flow ratio. At subsonic flight Mach numbers the inlet was unaffected by angles of attack or yaw between 0° and $9\frac{1}{2}^O$, as shown in figure 21.

The compressor-inlet total-pressure contours shown in figure 22 were selected near the engine matching condition. The pressure distribution changed gradually for Mach numbers 0.66 to 2.1 and was not markedly altered by angles of attack or yaw. At engine matching conditions the level of distortion varied from 7.0 to 5.5 percent between Mach numbers of 1.5 and 2.0.

<u>Summary of stability limits</u>. - Sufficient stable mass-flow-ratio range was attained (shown in fig. 23 as lines of min. stable weight flow) to satisfy engine idle or windmill requirements at Mach numbers 1.5 and 1.7 except for a yaw angle of 6°. At Mach numbers 1.9 and 2.0, except for angles of attack of 2^O to 5° at $M_0 = 1.9$, unstable flow occurred at engine rotative speeds somewhat greater than idle. Opening the bypass to the largest setting, S_5, resulted in ample stable range at an angle of attack of 2^O at Mach numbers 2.1 and 2.0. Similar increases can be anticipated at other angles of attack and yaw.

<u>Incremental axial-force coefficients</u>. - Because of the asymmetric nature of the model, only incremental axial-force coefficients due to normal-shock spillage are presented. The curves shown in figure 24 can be used for any configuration when adjusted for changes in critical mass-flow ratio caused by ramp bleed. This is possible since the force due to all ducted airflow (bypass configurations excluded) was removed from the force coefficient. As shown in figure 24, the slopes of the incremental axial-force curves changed only slightly with Mach number. Although not shown, the slopes were not significantly changed by angles of attack or yaw. With the vent installed and without removing the momentum change of the vent air (since the mass flow was not known), the variations of axial-force coefficient were within ±0.005 of the no-vent values at Mach number 2.0.

In order to interpret the magnitude of the slopes of the force-coefficient curves, slopes for both normal- (open-nose inlet) and oblique-shock spillage for a sharp-lip inlet are included in figure 24.

The slopes of the two additive-drag curves have been drawn through the point of zero incremental experimental drag for comparison. (For this inlet excessive internal contraction results in a critical mass-flow ratio less than that for oblique-shock spillage only.) The spillage drag comparison indicates that the experimental values are approximately equivalent to those for an open-nose inlet. The possible reductions in spillage drag attainable by bypassing air in excess of engine requirements are indicated for Mach number 2.0.

Effective-thrust-ratio comparison. - Airflow and thrust characteristics for a conventional turbojet engine with afterburner were used for computing the ratio of net thrust minus spillage drag to ideal thrust with convergent nozzle (referred to hereinafter as the effective thrust ratio). For bypass setting S_1, which approximates a particular ejector pumping capacity for optimum net thrust gains, a net thrust increase of 8 percent was assumed at Mach number 2.0.

The combined effect of increased thrust due to the ejector and decreased spillage drag amounts to 10 percent of the ideal convergent-nozzle thrust, as shown in figure 25 for bypass setting S_1. Further reductions in spillage drag are possible by increasing bypass mass-flow ratio. However, since the ejector is probably not capable of pumping this increased amount of flow at optimum net-thrust gain, a separate bypass exit for exhausting directly to the external stream, the difference between S_1 and S_5 (bypass mass-flow ratio of 0.155), could be used for the peak thrust condition. (S_5 and the exit-type bypass could then be used together for reduced engine speed.) For an exit-type bypass, a spillage-drag reduction on the order of 80 percent is possible (ref. 2). This would give an effective thrust ratio of 0.80 compared with 0.70 for S_1, which amounts to an improvement of 10 percent of ideal convergent-nozzle thrust or an increase of 14.2 percent over the S_1 value.

SUMMARY OF RESULTS

A side inlet having a fixed 12° two-dimensional compression surface was tested at Mach numbers of 0.66 and 1.5 to 2.1, angles of attack between $-2\frac{1}{2}^\circ$ and $9\frac{1}{2}^\circ$, and angles of yaw from $2\frac{1}{2}^\circ$ windward to 6° leeward. The conical nose of the fuselage was canted downward $3\frac{1}{2}^\circ$ relative to the horizontal axis and the inlet was canted downward $7\frac{1}{4}^\circ$. Other features of the air induction system included internal contraction in excess of starting limits, a low-angle rounded-lip cowl, a long constant-area

section followed by overexpansion and contraction between the diffuser exit and the compressor inlet, and a flush-slot annular bypass. A somewhat systematic investigation was made of perforations and slots for compression-surface bleed. The following results were obtained:

1. At Mach numbers of 2.0 and 1.7, shock-induced separation of the ramp boundary layer was unsteady and resulted in a large static-pressure fluctuation at the diffuser exit without the usual normal-shock type of inlet buzz. This limited the usable stable mass-flow-ratio range (from critical) to 0.10 and 0.12 and peak total-pressure recovery to 0.802 and 0.91 at Mach numbers 2.0 and 1.7, respectively. At Mach number 1.5, separation was not evident, the peak recovery was 0.96, and the stable mass-flow range was 0.33.

2. External (ramp) or internal (throat) perforations or slots partially reduced and stabilized the shock-induced separation. Increased peak pressure recoveries and equal or better stability ranges were obtained for all configurations. Generally, peak recovery occurred just before minimum stable flow conditions; and, hence, the configuration having the greatest stability tended to have the highest peak recovery. At Mach number 1.5, where separation was not significant, ramp or throat bleed also increased peak recovery and stable range.

3. External perforations in the region of the shock lambda gave the greatest increases in stable range and peak recovery. At Mach number 2.0 the perforated ramp having the largest hole flow area and distribution (7.7 percent of ramp surface area or 11.5 percent of capture area) gave the highest peak recovery of 0.89 and a stable mass-flow range of 0.278. Maximum bleed flow at peak recovery was somewhat in excess of 6 percent of the flow that entered the inlet.

4. The distribution and density of the bleed flow area were important factors. For example, another configuration having the same size of holes but only 60 percent of the flow area of that above (4.5 percent of ramp surface area or 6.7 percent of capture area) gave a peak pressure recovery of 0.87 and a stability range of 0.285. The largest external slot in the same general region of the ramp (4.9 percent of ramp surface area or 7.3 percent of capture area) had a peak recovery of 0.85 and a stable range of 0.17.

5. Although internal slots in the region of the throat resulted in a less stable range than external bleed, the envelope of pressure recoveries between critical and minimum stable flow was higher. This occurred because of greater bleed mass flow, since the terminal shock was always ahead of the bleed slot.

6. The long duct section between the diffuser exit and the compressor inlet was very effective in reducing large values of distortion.

With the solid ramp a distortion of 32 percent was reduced to 10.5. The loss in total-pressure recovery was 4 percent or less, depending on mass-flow ratio. With throat bleed, distortion was considerably less at the diffuser exit and only slightly reduced by the long duct.

7. A flush-type bypass near the compressor inlet tended to offset the total-pressure loss due to the long duct section by bleeding off the boundary layer generated therein.

8. Both the solid and perforated ramp inlets had excellent angle-of-attack characteristics, which may be attributed to the standing bow wave due to excessive contraction, rounded cowl lips, generous fillets, and the canting of the nose and inlet. At Mach number 2.0 the total-pressure recovery at critical flow varied only 3 percent of free-stream total pressure for angles of attack from 0° to $9\frac{1}{2}^{\circ}$. The highest level of pressure recovery occurred near 5° angle of attack when the body flow field was nearly alined with the inlet axis.

Lewis Flight Propulsion Laboratory
    National Advisory Committee for Aeronautics
        Cleveland, Ohio, October 8, 1956

REFERENCES

1. Sterbentz, William H.: Factors Controlling Air-Inlet Flow Distortions. NACA RM E56A30, 1956.

2. Allen, J. L., and Beke, Andrew: Performance Comparison at Supersonic Speeds of Inlets Spilling Excess Flow by Means of Bow Shock, Conical Shock, or Bypass. NACA RM E53H11, 1953.

TABLE I. - RAMP BLEED CONFIGURATIONS

Configuration	Flow area, A_b, sq in.	A_b/A_R	A_b/A_{th}	A_b/A_c
External perforations:				
A_1	0.52	0.0086		0.013
A_2: Same as A_1 with increased hole size	1.16	.019		.028
A_3: Same as A_2 plus duplicate pattern aft to cowl lip	2.29	.038		.056
A_4: Same as A_3 plus 5 rows of 1/8" holes forward	3.82	.063		.093
A_5: Similar to A_4, all 1/16" holes	2.08	.034		.051
A_6: Same pattern as A_5, front 12 rows 3/32" holes	3.47	.057		.085
A_7: Same pattern as A_5, all 3/32" holes	4.69	.077		.115
A_8: Different pattern, all 3/32" holes	2.74	.045		.067
External slots:				
B_1: 0.10" Slot	0.64	0.015		0.0157
B_2: 0.25" Slot	1.60	.026		.039
B_3: 0.50" Slot	3.00	.049		.073
Internal slots:				
C_3: 0.50" Slot	3.00		0.134	0.039
C_4: 0.72" Slot, changed ramp contour	4.59		.205	.11
Internal perforation:				
D_1: Same as A_1, but 1" inside cowl	0.52			0.013
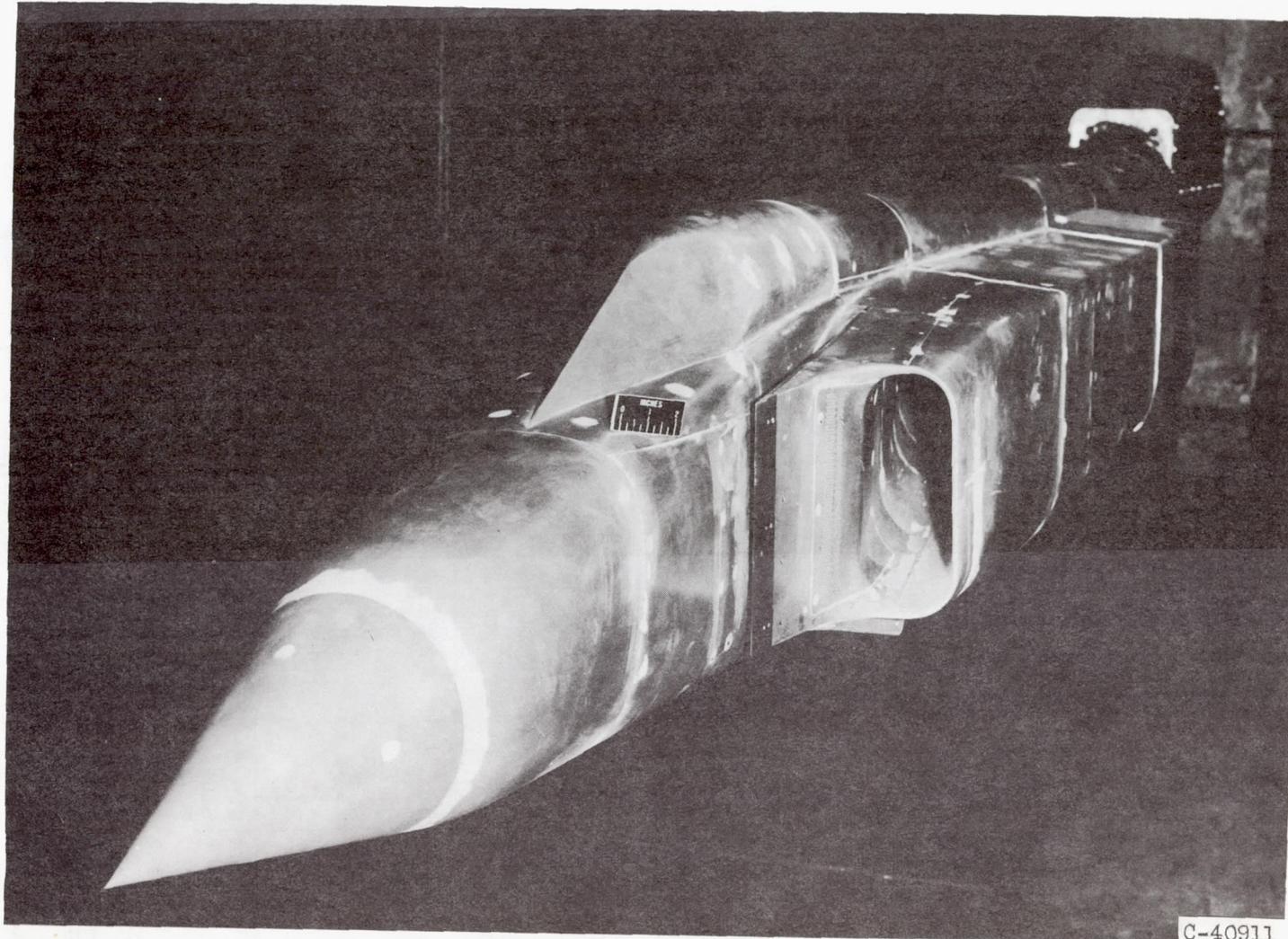
(a) Three-quarter front view.

Figure 1. - Photographs of model with A_8V ramp.

4186

Vent for ramp
bleed flow

C-40888

(b) Side view.

C-40887
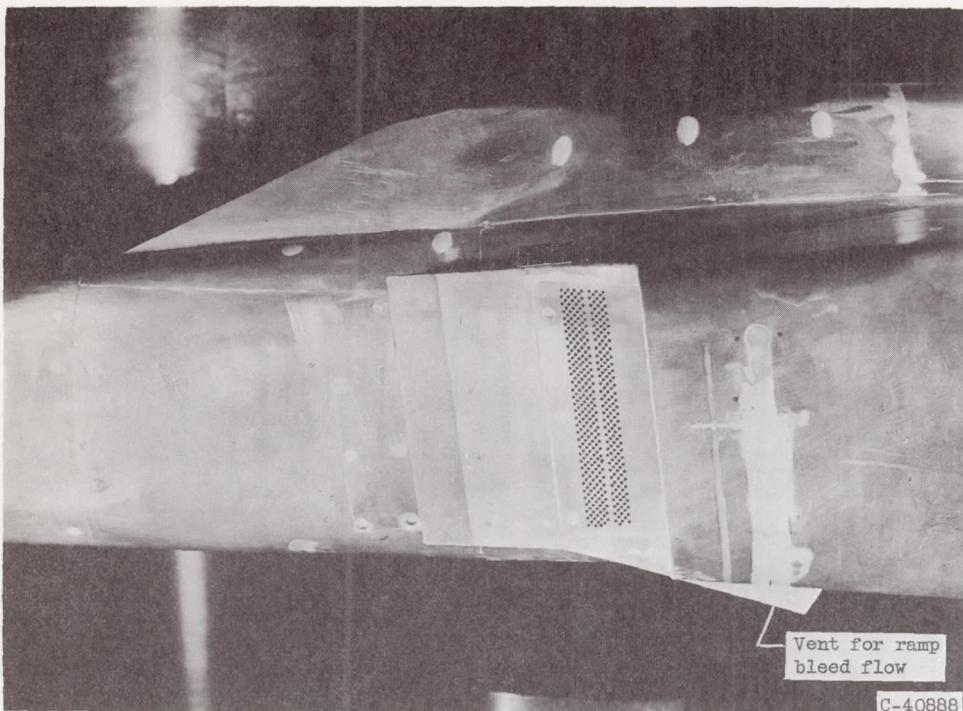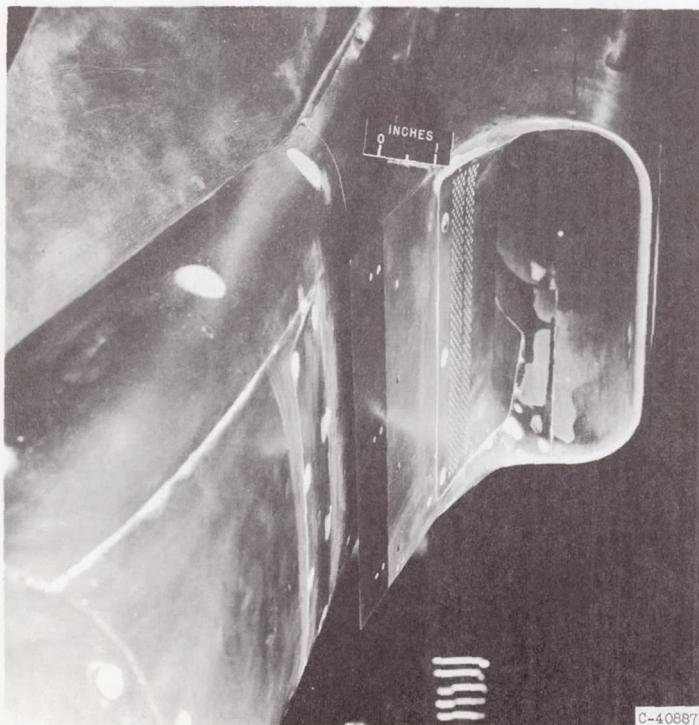
(c) Closeup view of inlet.

Figure 1. - Concluded. Photographs of model with A_8V ramp.

Strain-gage
balance

Sting for mounting
to support strut

3 Mass-flow
control plugs

30°

A

A

A

Fixed 12° compression ramp

Sting

Boundary-layer-
diverter air duct

Main
duct

Adjustable bypass slot

Ramp bleed-
air duct

Section B-B

Detail C: Bypass slot, accessory
bullet, and compressor-face rake

Ramp bleed
ducting

B

Wind-
shield

3° 30'

7° 15'

8° 45'

2° 35'

B

Boundary-layer-
diverter airscoop

Constant-area section

CD-5320

Station

2

Inlet
throat

3

Diffuser
exit

4

Compressor
face

Section A-A

-10   0   10   20   30   40   50   60   70   80   90   100   110   120   Inches

Figure 2. - Schematic sketch of model.
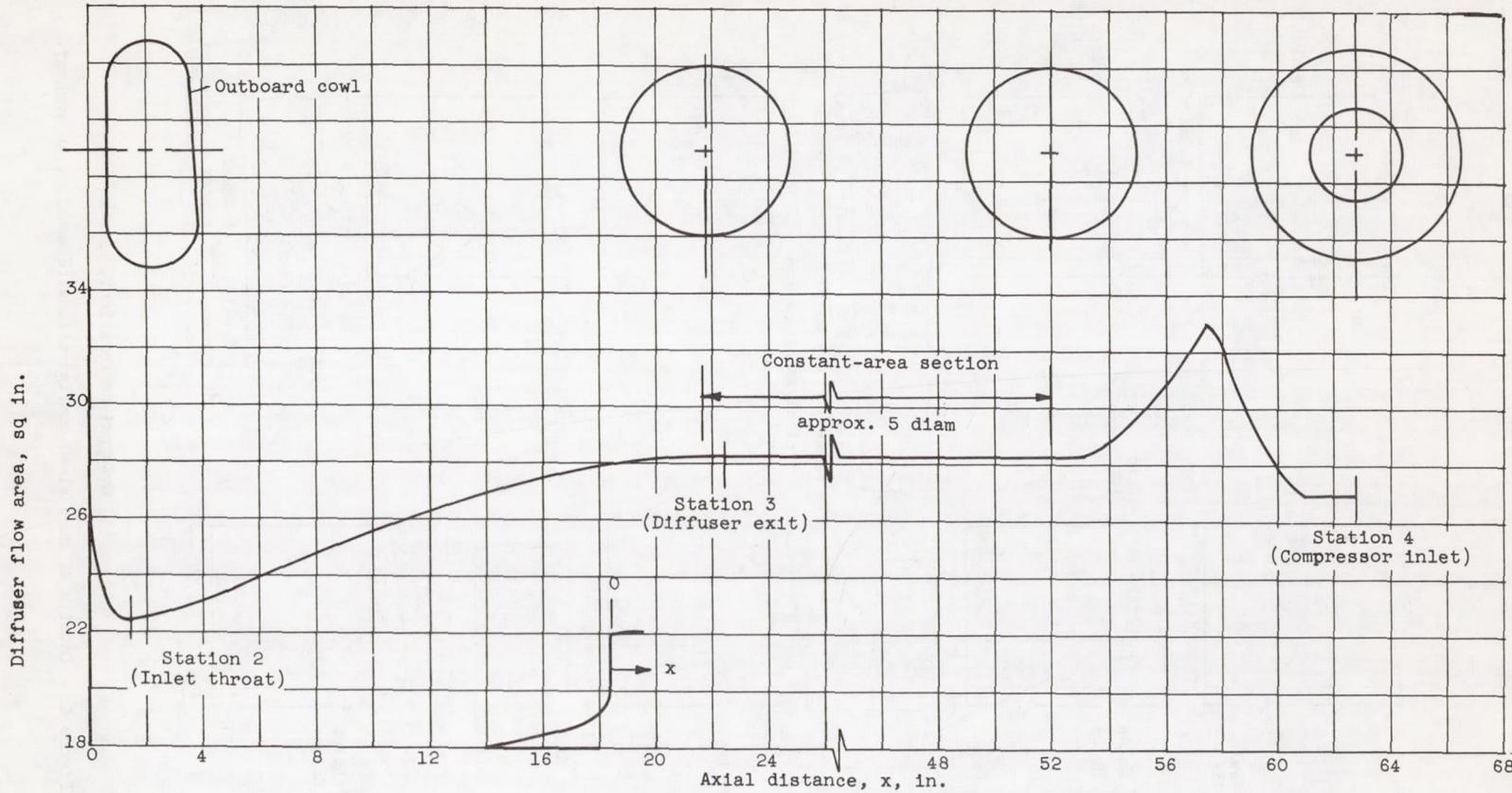
Figure 3. - Diffuser area variation.
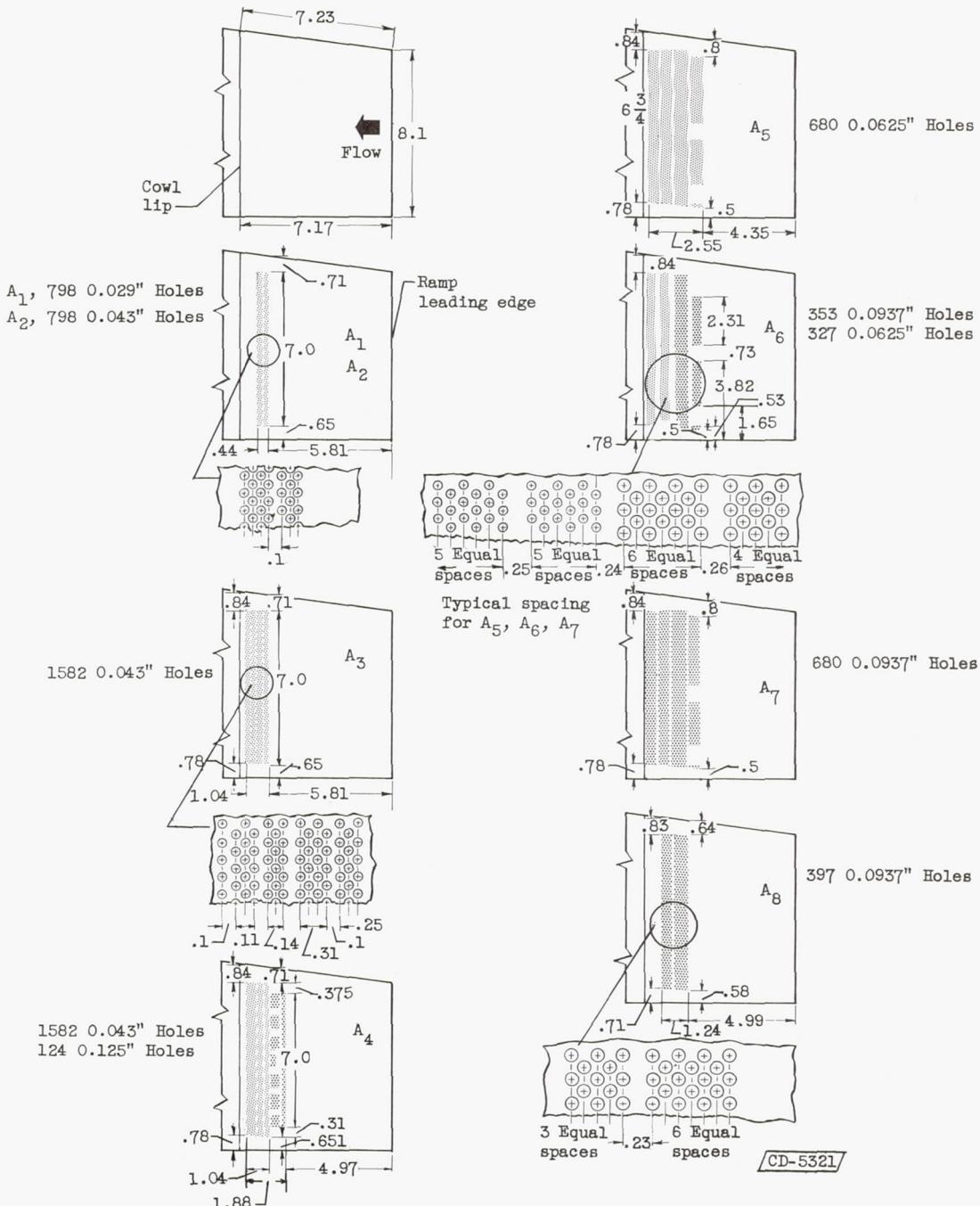
(a) External perforations.

Figure 4. - Details of ramp bleed configurations (dimensions in inches).

CH-4   4186

Typical external
slot

1.3

6

C₃

C₄V

Horizontal axis

1.4

Throat,
except C₄V

0.1   Cowl lip
45° |← 1 →|

B₁
                                    Bleed chamber

0.25   Cowl lip
45° |← 1 →|

B₂

0.5   Cowl lip
1 1/8
45°

B₃

0.5   Cowl lip
.9
45°

C₃

Cowl lip   1.44
.72

C₄V   CD-5322
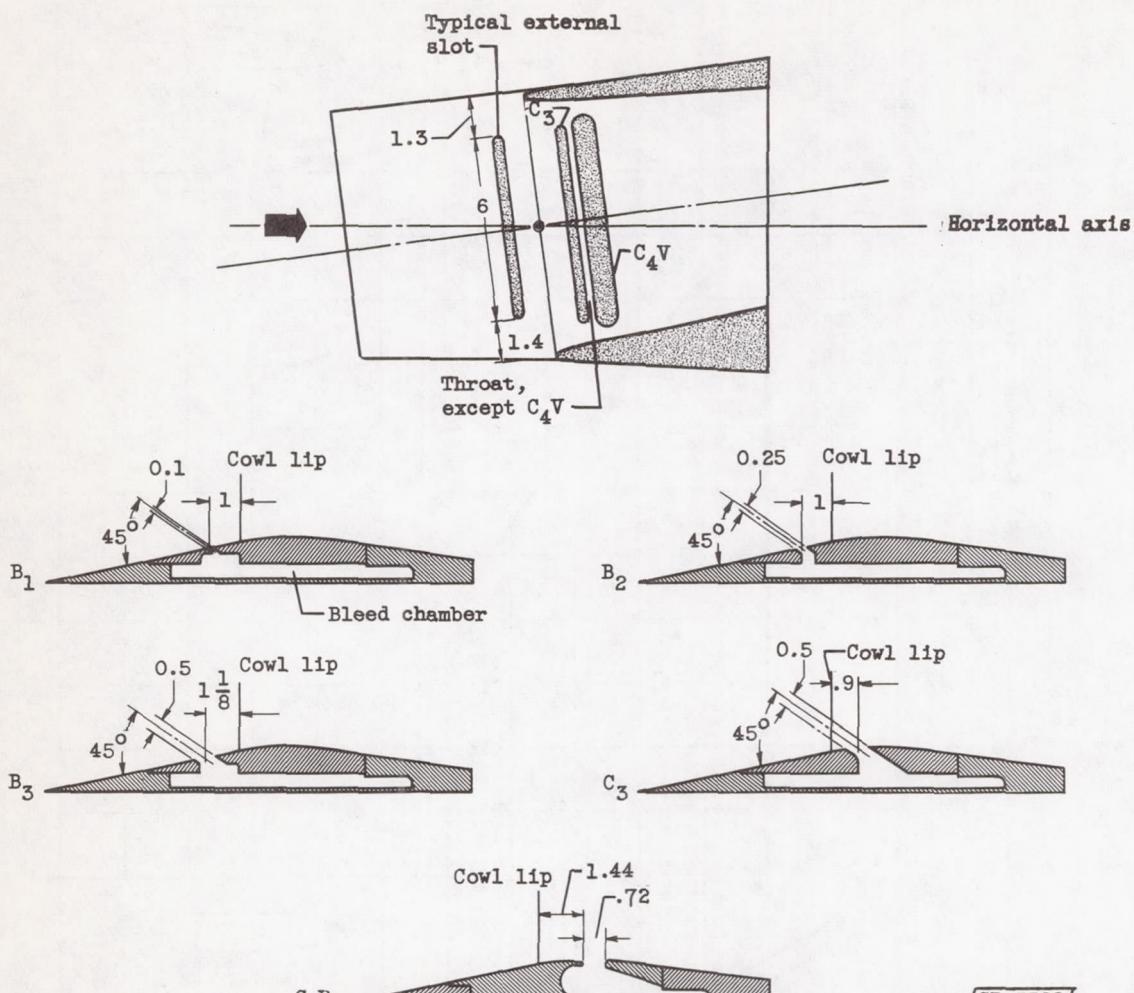
(b) Bleed slots.

Figure 4. - Concluded. Details of ramp bleed configurations (dimensions in inches).
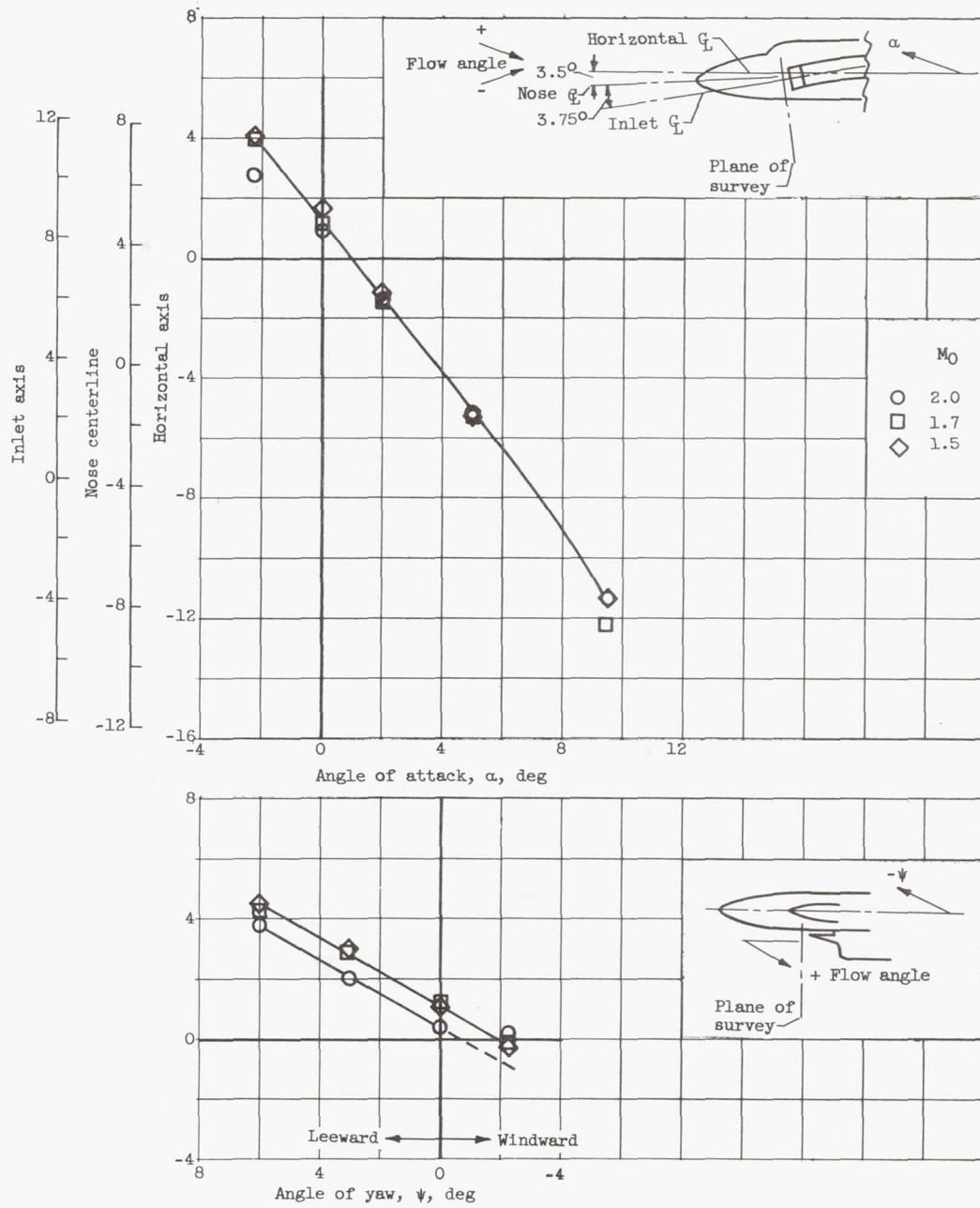
Figure 5. - Flow field approaching inlet.

CH-4 back   4186
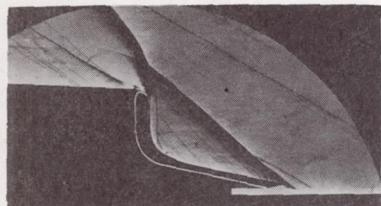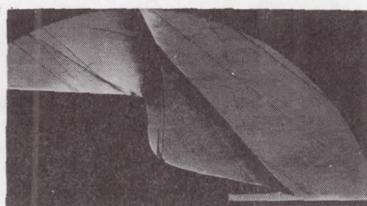
$\frac{m_4}{m_0} = 0.773$

$\frac{m_4}{m_0} = 0.676$
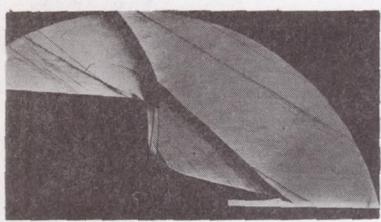
$\frac{m_4}{m_0} = 0.744$
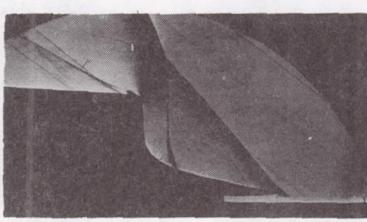
$\frac{m_4}{m_0} = 0.623$
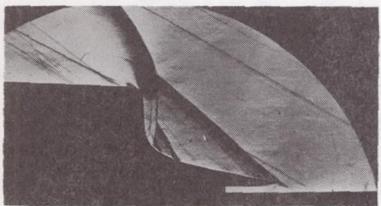
$\frac{m_4}{m_0} = 0.713$

$\frac{m_4}{m_0} = 0.553$
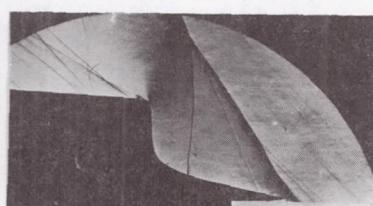
$\frac{m_4}{m_0} = 0.573$
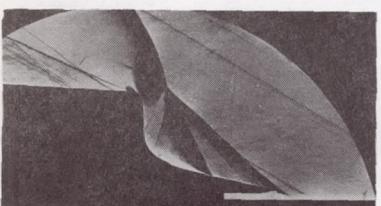
$\frac{m_4}{m_0} = 0.587$
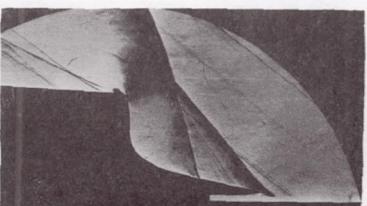
$\frac{m_4}{m_0} = 0.482$

$\frac{m_4}{m_0} = 0.297$

C-43056

(a) $M_0 = 2.0$.

(b) $M_0 = 1.7$.

(c) $M_0 = 1.5$.

Figure 6. - Schlieren photographs of solid-ramp inlet. Zero angle of attack.
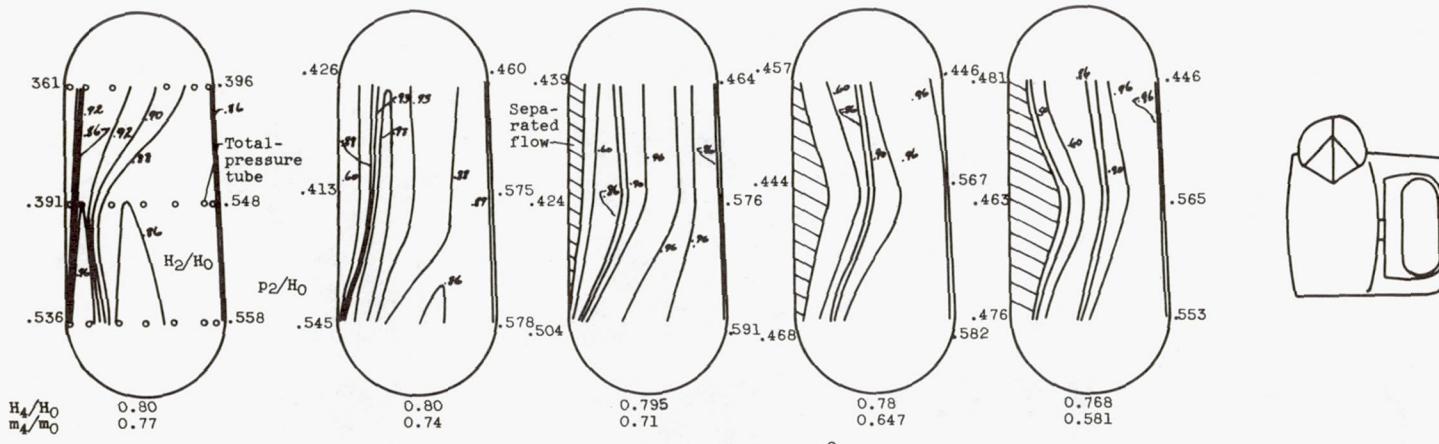
(a) Flight Mach number, 2.0; angle of attack, 0°.
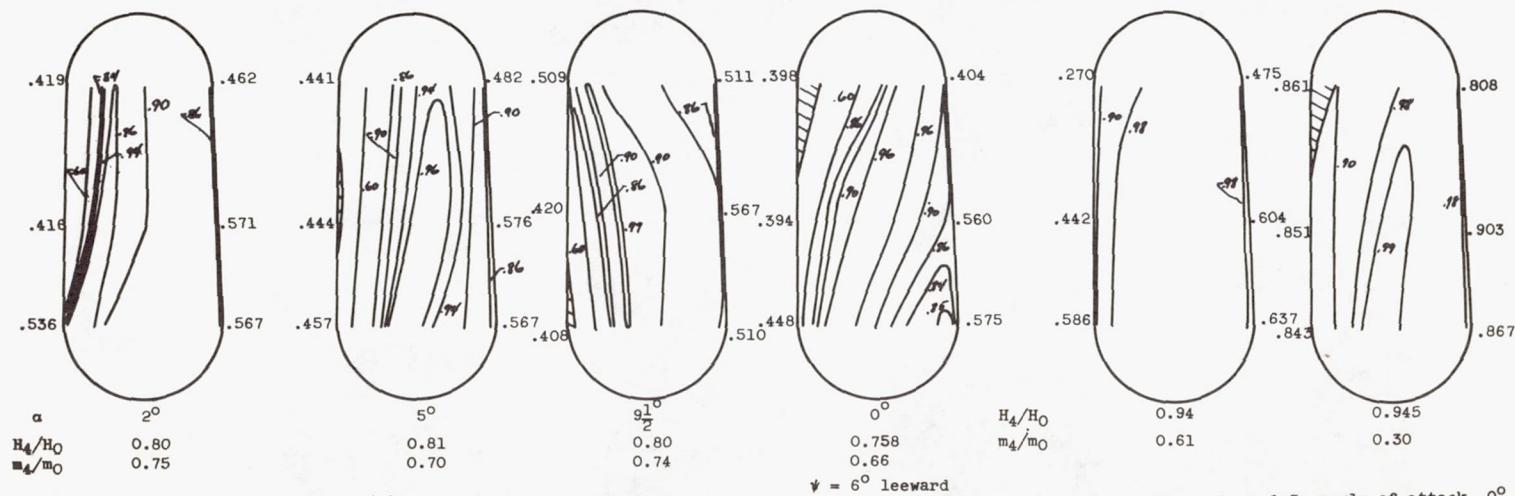
(b) Flight Mach number, 2.0.

(c) Flight Mach number, 1.5; angle of attack, 0°.

Figure 7. - Total-pressure contours $1\frac{1}{2}$ inches aft of cowl lip. Solid ramp.
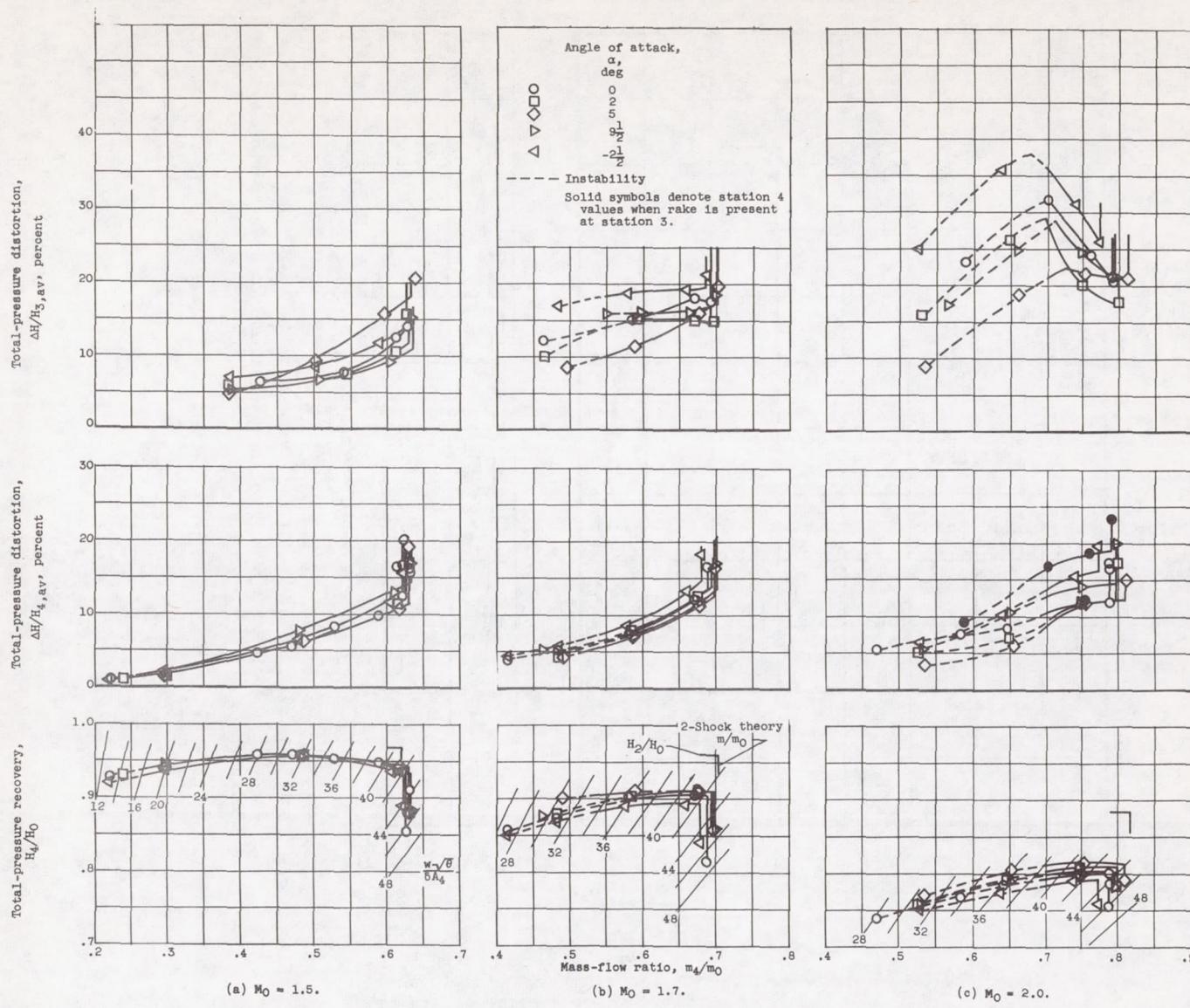
Figure 8. - Effect of angle of attack on inlet performance. Solid ramp.

(d) $M_0 = 0.66$.
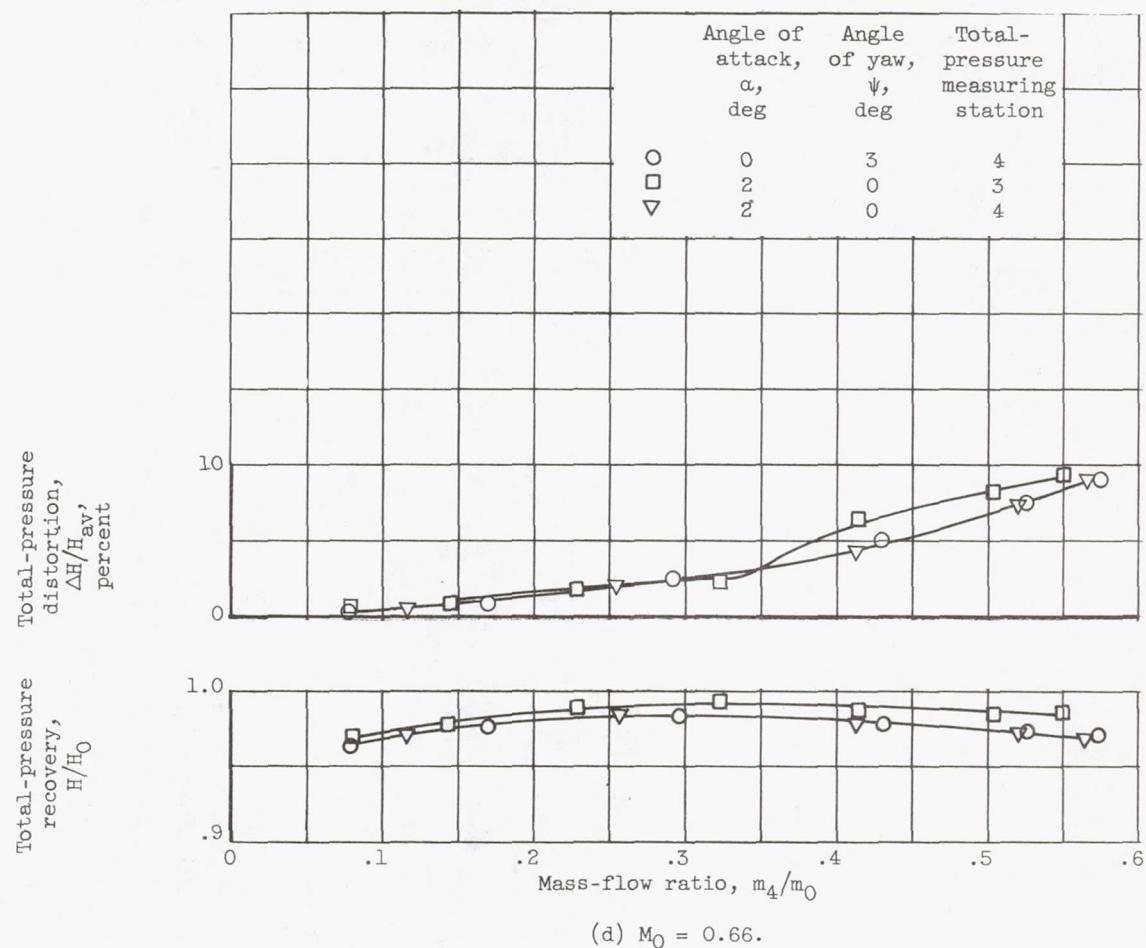
Figure 8. - Concluded. Effect of angle of attack on inlet performance.
Solid ramp.
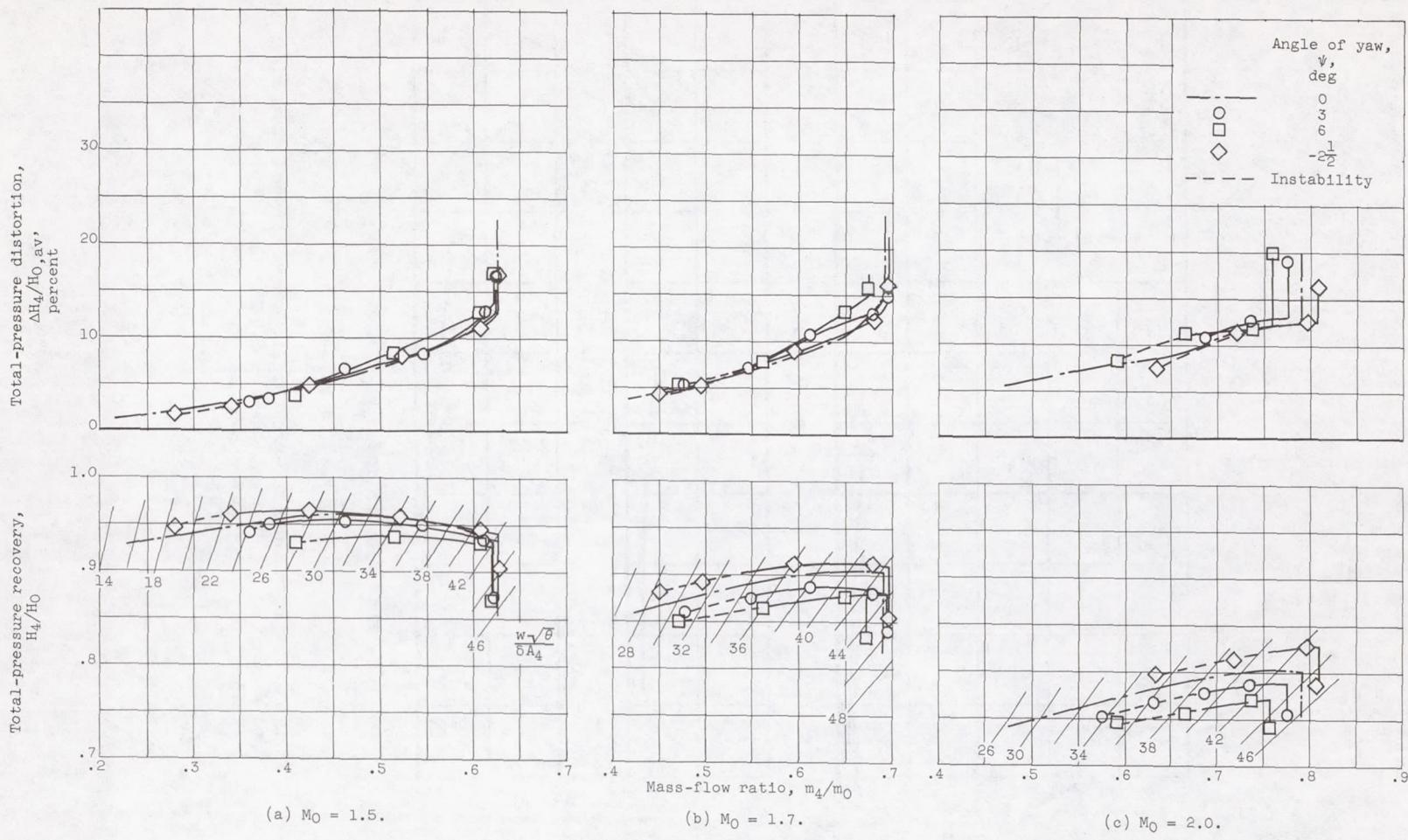
Figure 9. - Effect of yaw angle on inlet performance. Solid ramp.
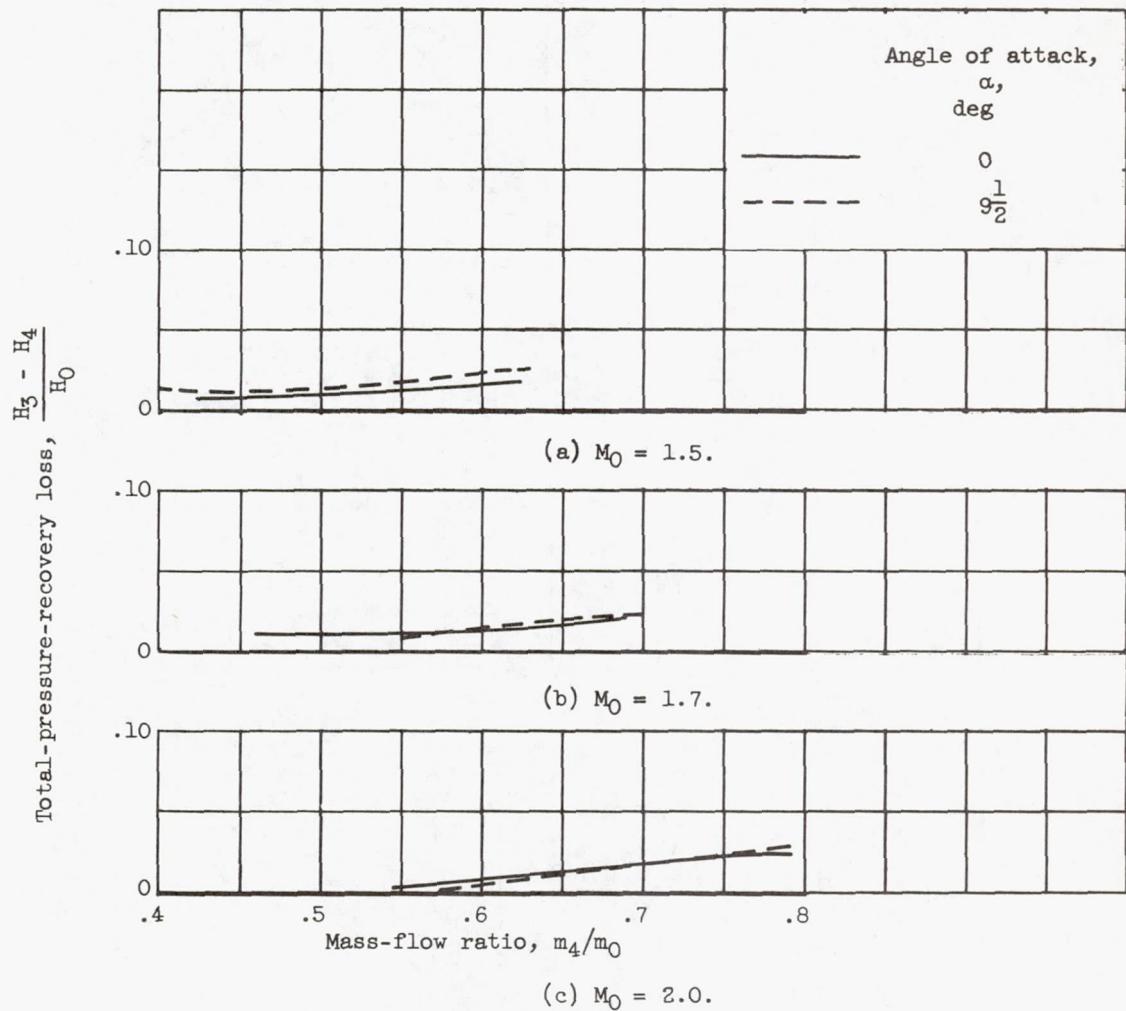
Figure 10. - Loss in total-pressure recovery between stations 3 and 4.
Solid ramp.

M_O	2.0	1.7	1.5	0.66
α	0°	0°	0°	2°
H_3/H_O	0.823	0.919	0.957	0.985
m_3/m_O	0.763	0.669	0.610	0.502
$\Delta H/H_{3,av}$	24%	18.4%	12.4%	9.2%

(a) Station 3.

M_O	2.0	1.7	1.5	0.66
α	0°	0°	0°	2°
H_4/H_O	0.808	0.905	0.938	0.972
m_4/m_O	0.752	0.671	0.614	0.521
$\Delta H/H_{4,av}$	12.4%	12.5%	11.6%	7.3%
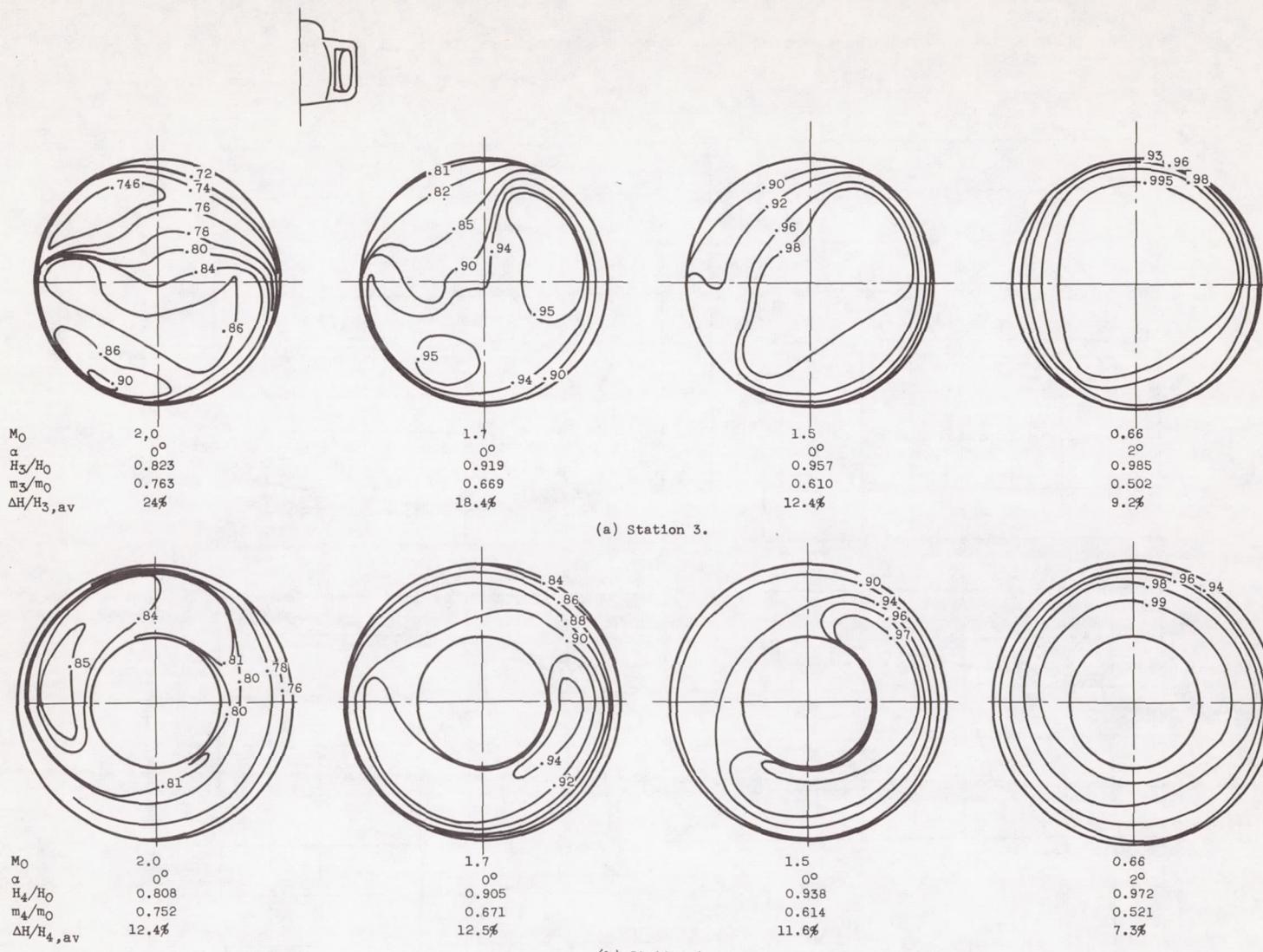
(b) Station 4.

Figure 11. - Comparison of total-pressure contours at duct stations 3 and 4. Solid ramp; yaw angle, 0°.

(a) Flight Mach number, 1.5.

(b) Flight Mach number, 2.0.
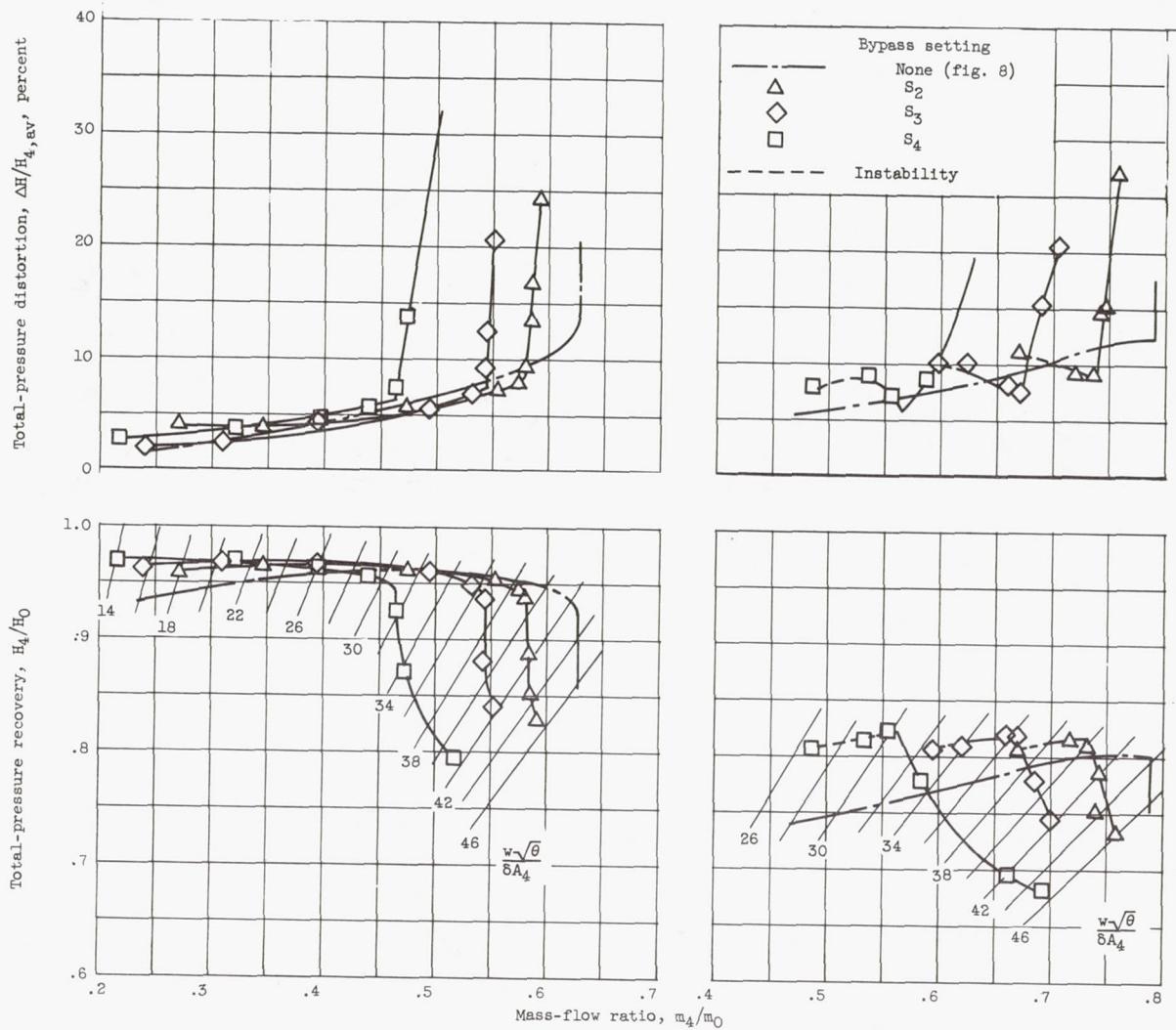
Figure 12. - Effect of bypass opening on inlet performance. Solid ramp; zero angles of attack and yaw.

Bypass setting: S_2
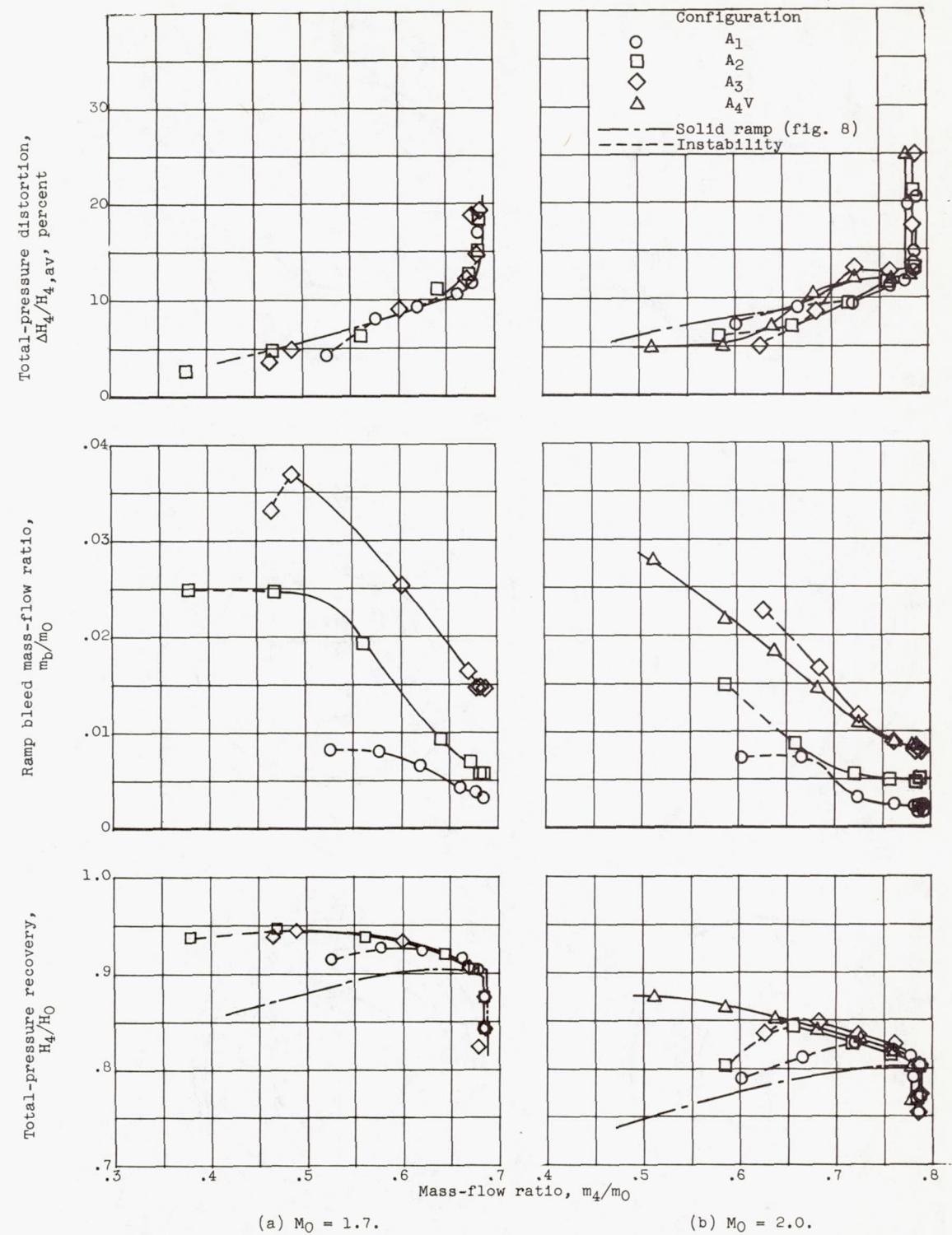
S_3

S_4

	S_2	S_3	S_4
H_4/H_O	0.952	0.959	0.957
m_4/m_O	0.553	0.496	0.440
$\Delta H/H_{4,av}$	7.1%	5.4%	5.6%

(a) Flight Mach number, 1.5.

	S_2	S_3	S_4
H_4/H_O	0.809	0.819	0.823
m_4/m_O	0.735	0.671	0.556
$\Delta H/H_{4,av}$	9.3%	7.9%	7.2%
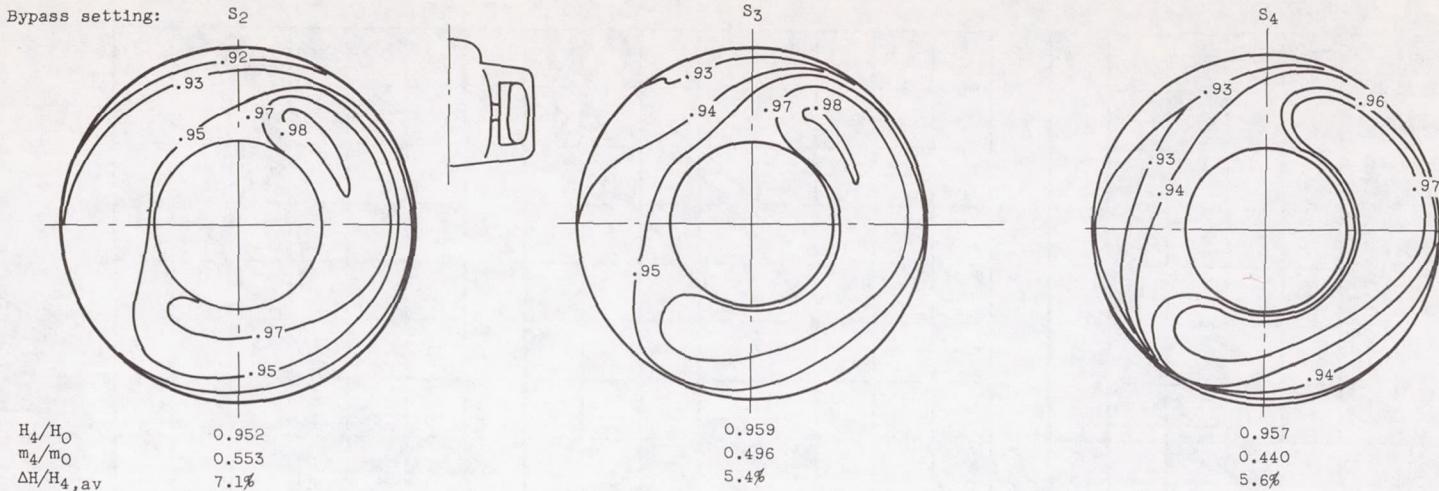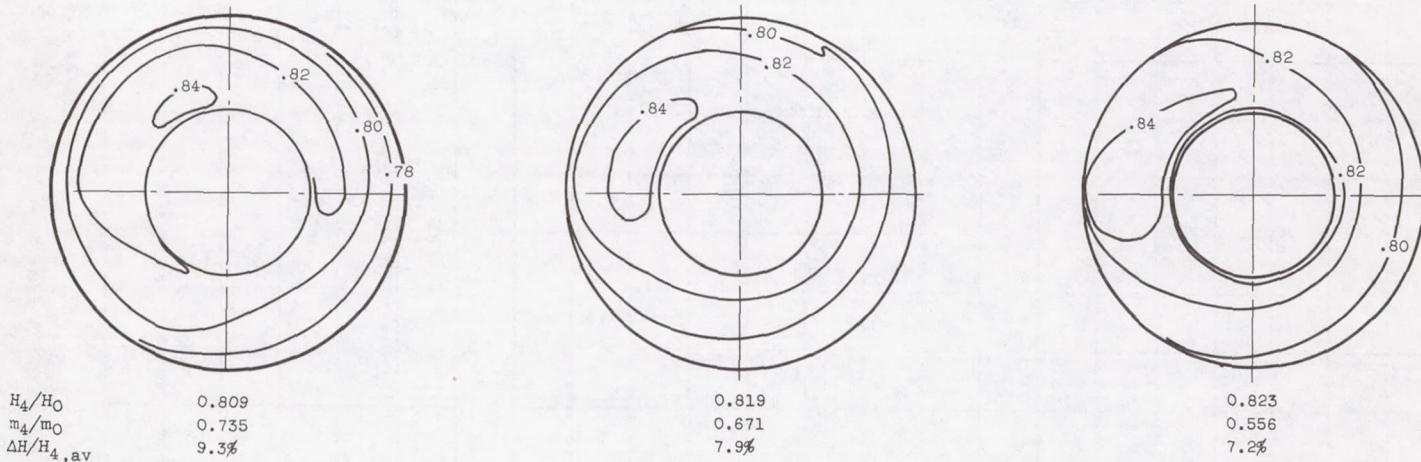
(b) Flight Mach number, 2.0.

Figure 13. - Effect of bypass opening on total-pressure contours at station 4. Solid ramp; zero angles of attack and yaw.

(a) $M_O = 1.7$.

(b) $M_O = 2.0$.

Figure 14. - Effect of external ramp perforations on inlet performance at zero angle of attack.

4186

(c) $M_0 = 2.0$.
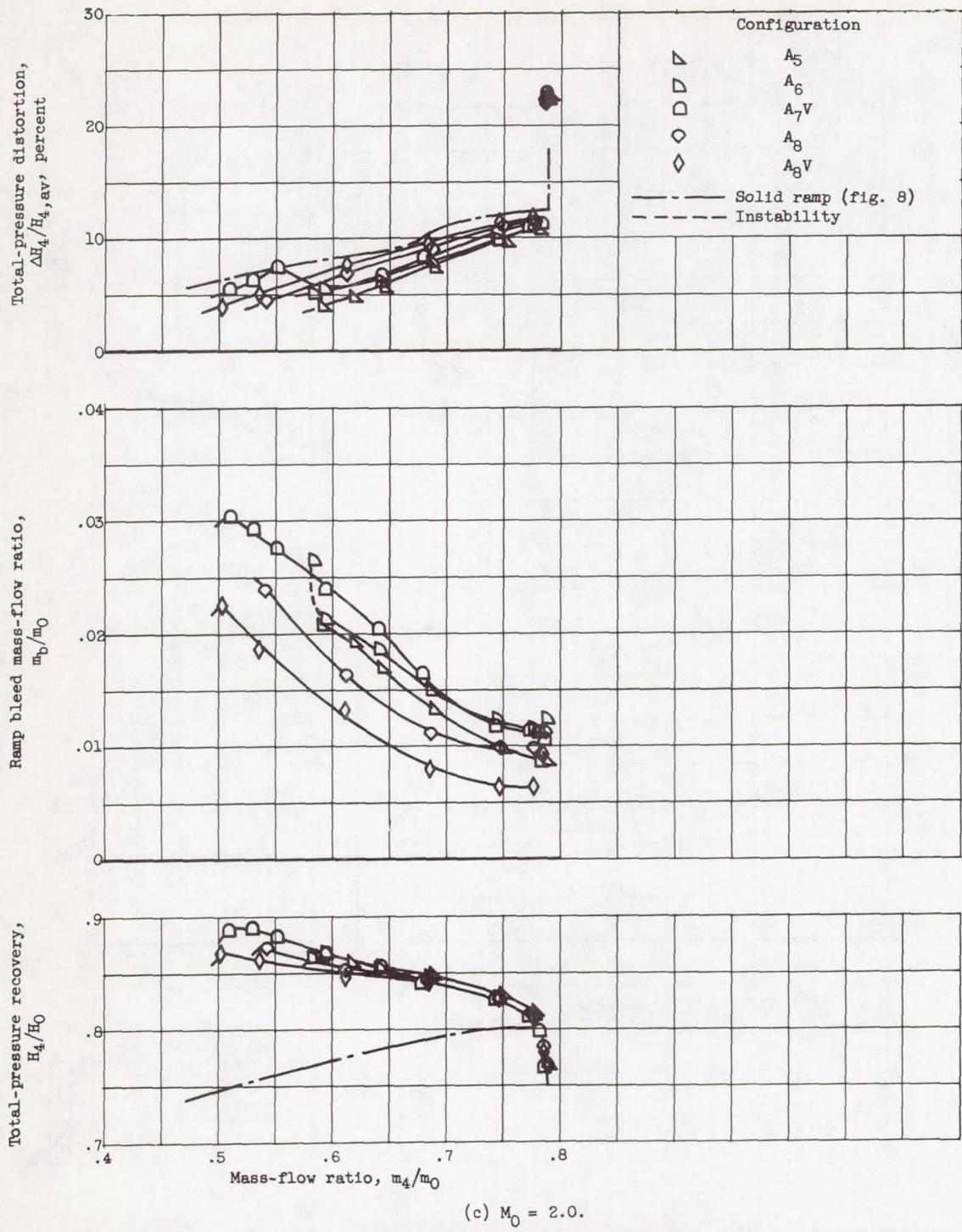
Figure 14. - Concluded. Effect of external ramp perforations on inlet performance at zero angle of attack.

(a) $M_O = 1.5$.

(b) $M_O = 1.7$.
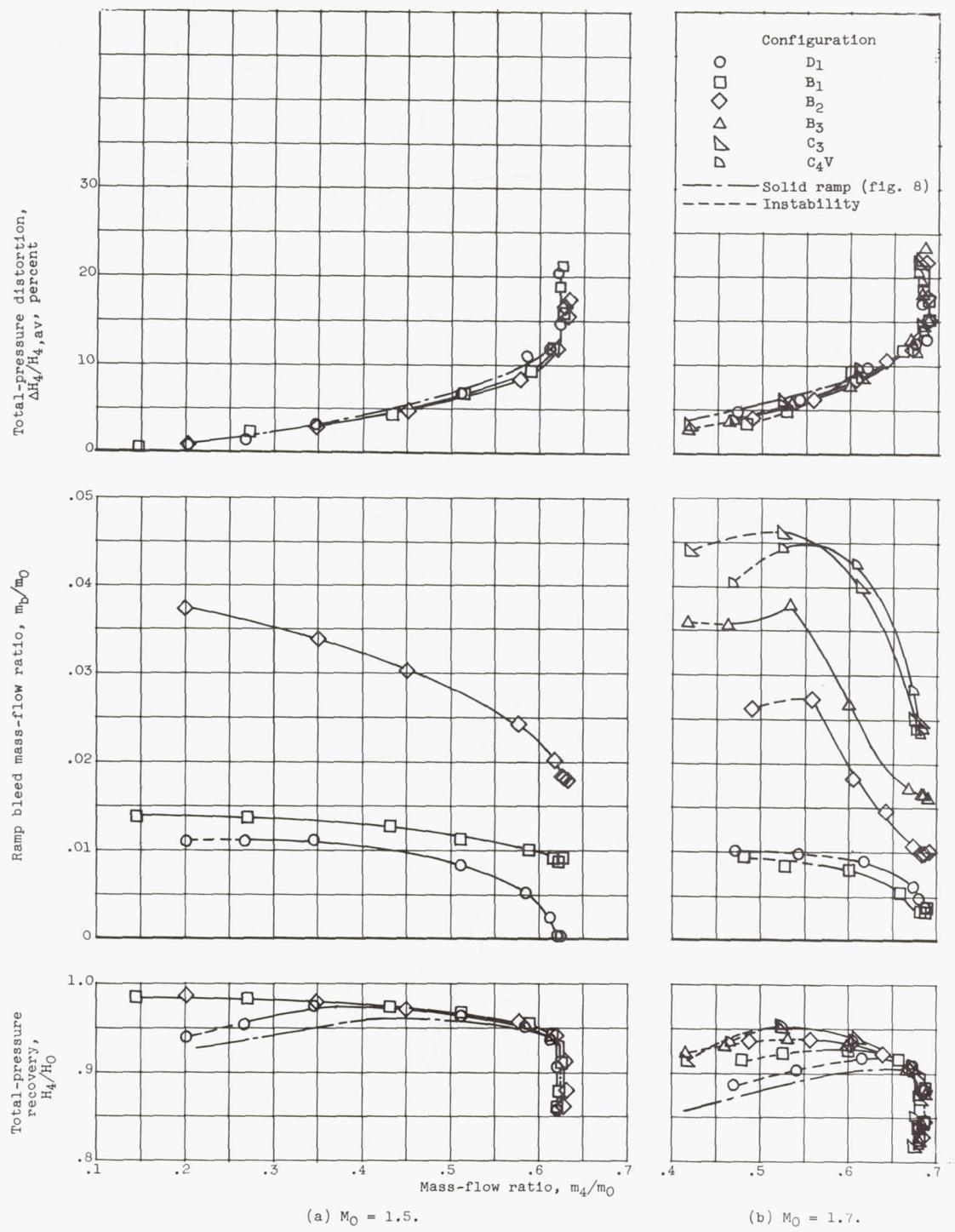
Figure 15. - Effect of external slots and internal slots and perforations on inlet performance at zero angle of attack.
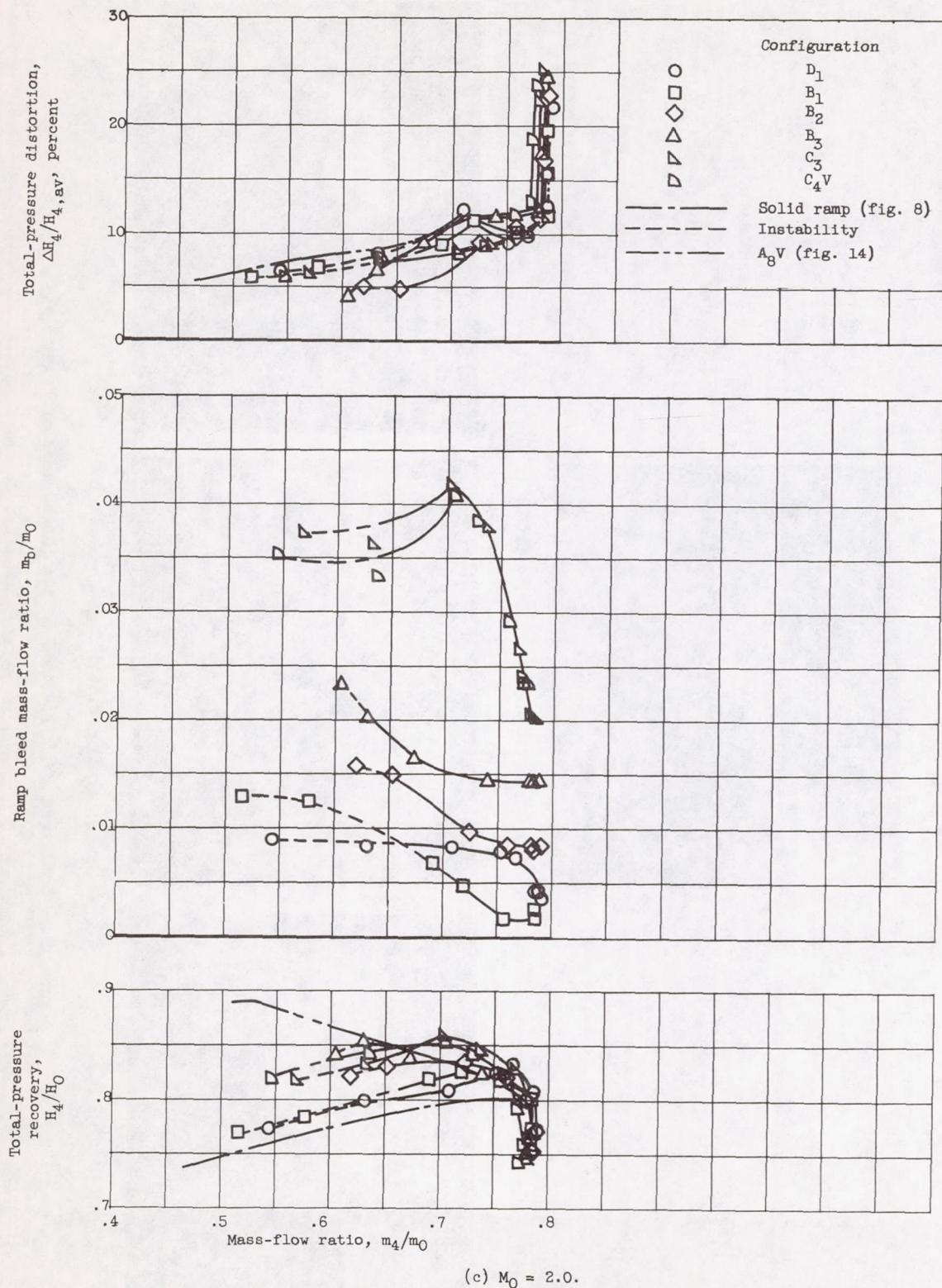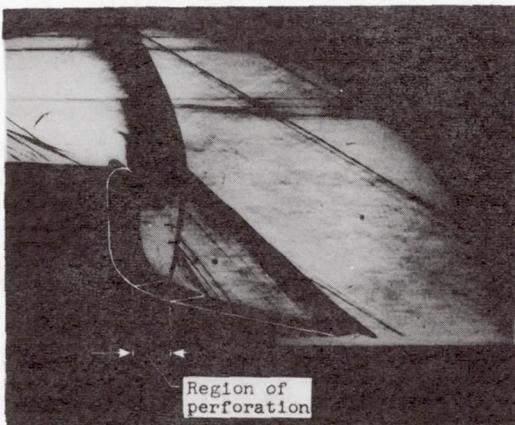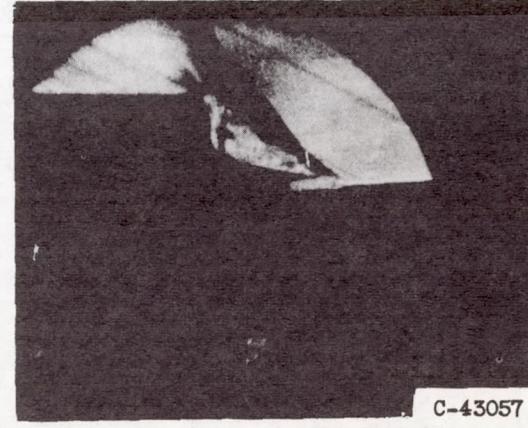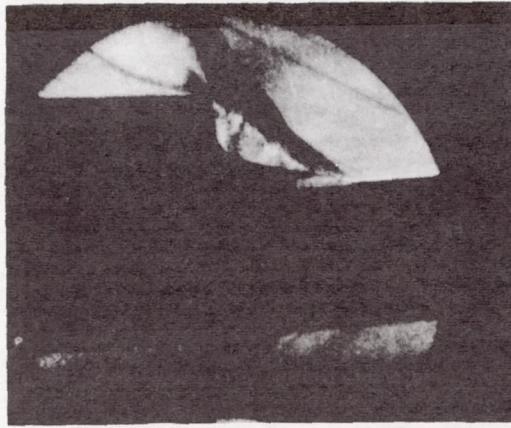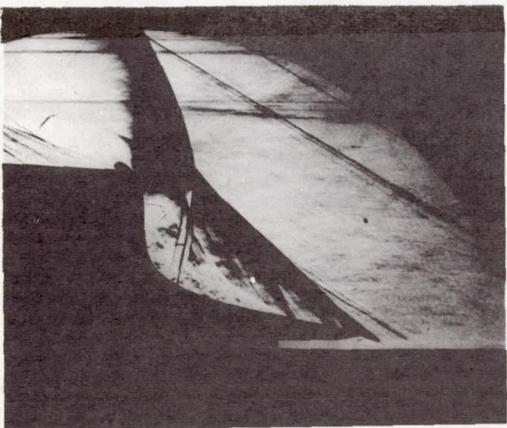
4186

(c) $M_O = 2.0$.

Figure 15. - Concluded. Effect of external slots and internal slots and perforations on inlet performance at zero angle of attack.

(a) $m_4/m_0 = 0.536$; $\Delta p_3/H_0 = 0.01$.

(b) $m_4/m_0 = 0.503$; $\Delta p_3/H_0 = 0.19$.

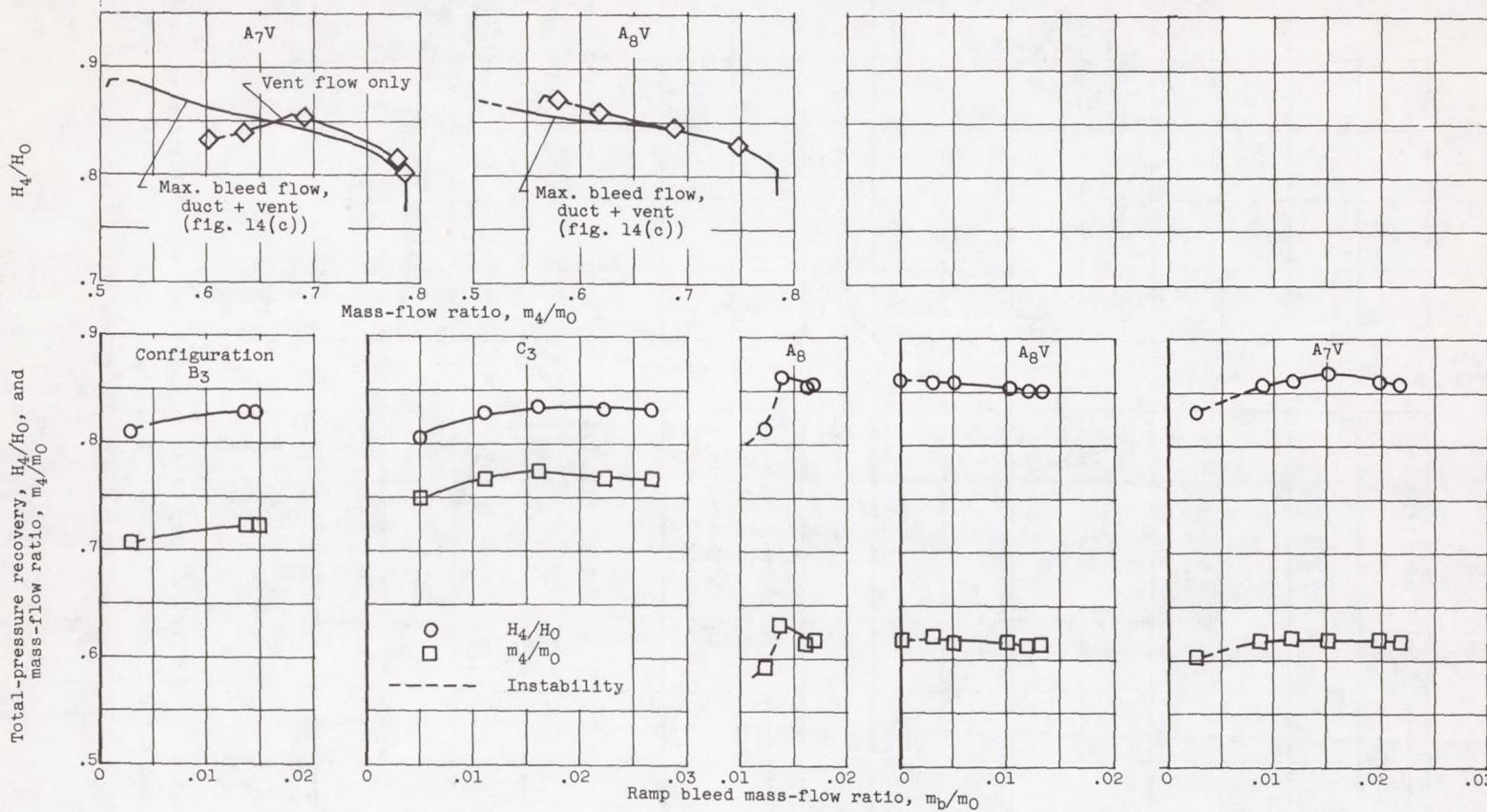Figure 16. - Schlieren and high-speed motion photographs of inlet A_8V.

Figure 17. - Some effects of varying bleed mass flow. Flight Mach number, 2.0; angle of attack, 0°.
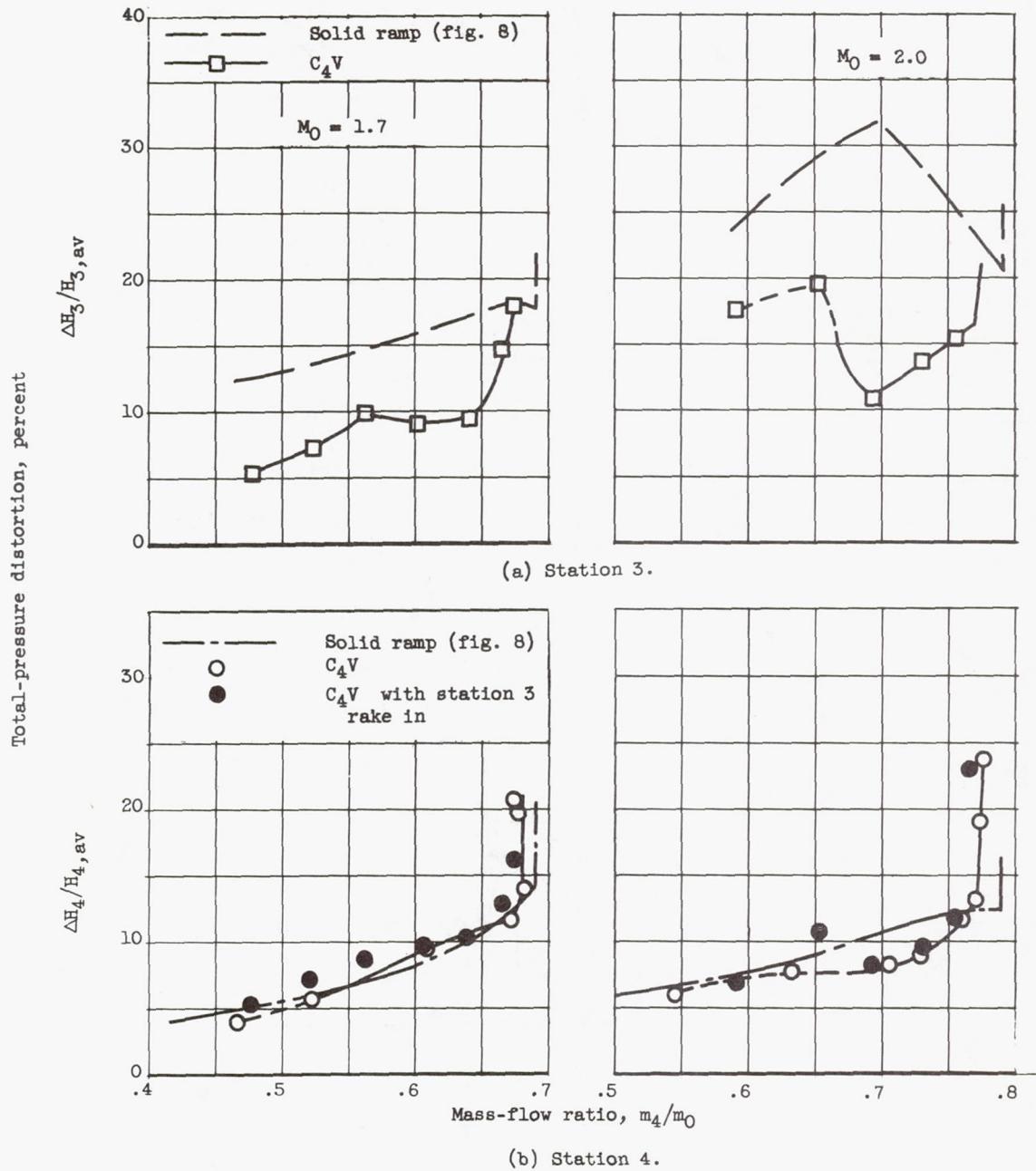
(a) Station 3.

(b) Station 4.

Figure 18. - Effect of ramp bleed on total-pressure distortion at stations 3
and 4 for configuration C_4V. Zero angle of attack.

(a) Flight Mach number, 1.5.

(b) Flight Mach number, 1.7.

Figure 19. - Effect of flight Mach number and angle of attack on inlet performance with A_8V perforated ramp and bypass setting S_1 (unless noted).

(c) Flight Mach number, 1.8; angle of attack, 2°.   (d) Flight Mach number, 1.9; angle of attack, 2°.
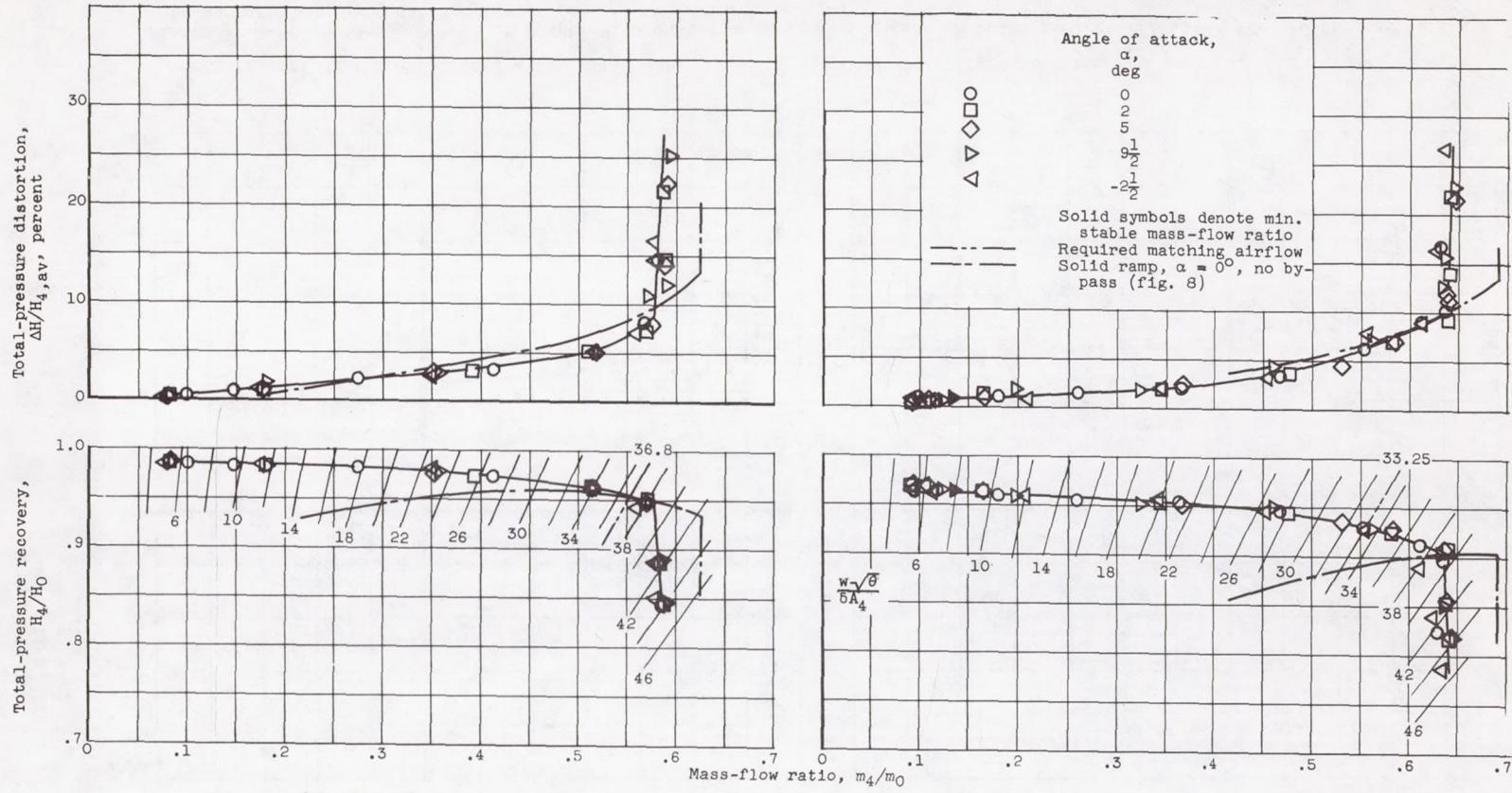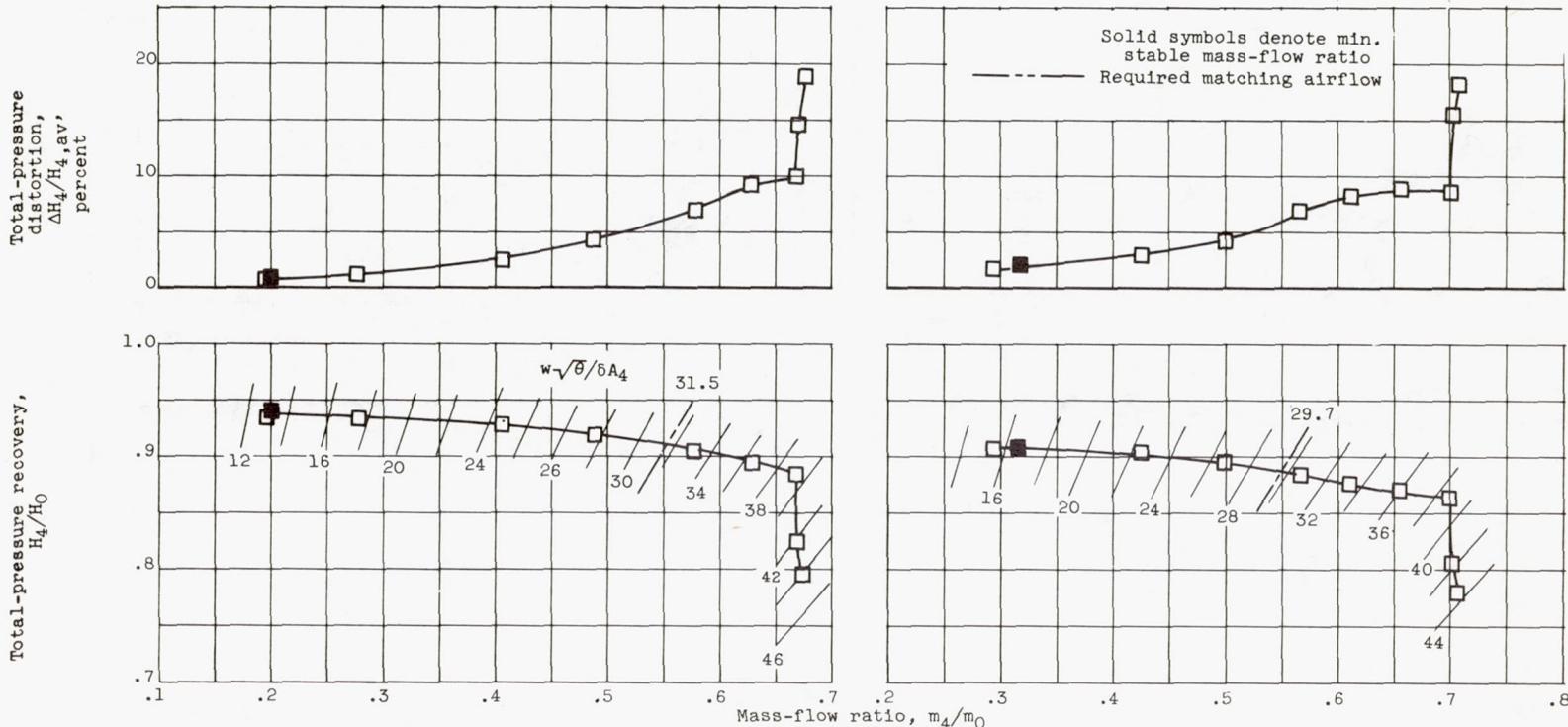
Figure 19. - Continued. Effect of flight Mach number and angle of attack on inlet performance with A_8V perforated ramp and bypass setting S_1 (unless noted).

Total-pressure distortion, $\Delta H_4/H_4$,av, percent

Total-pressure recovery, H_4/H_0

Angle of attack,
α,
deg

○ 0
□ 2
◇ 5
▷ $9\frac{1}{2}$
◁ $-2\frac{1}{2}$

----- Required matching airflow
—·—· Solid ramp, $\alpha = 0°$, no bypass
  (fig. 8)
Solid symbols denote min.
  stable mass-flow ratio
Tailed down symbols denote
  bypass setting S_5
Tailed up symbols denote
  zero bypass

$\frac{w\sqrt{\theta}}{\delta A_4}$

Mass-flow ratio, m_4/m_0

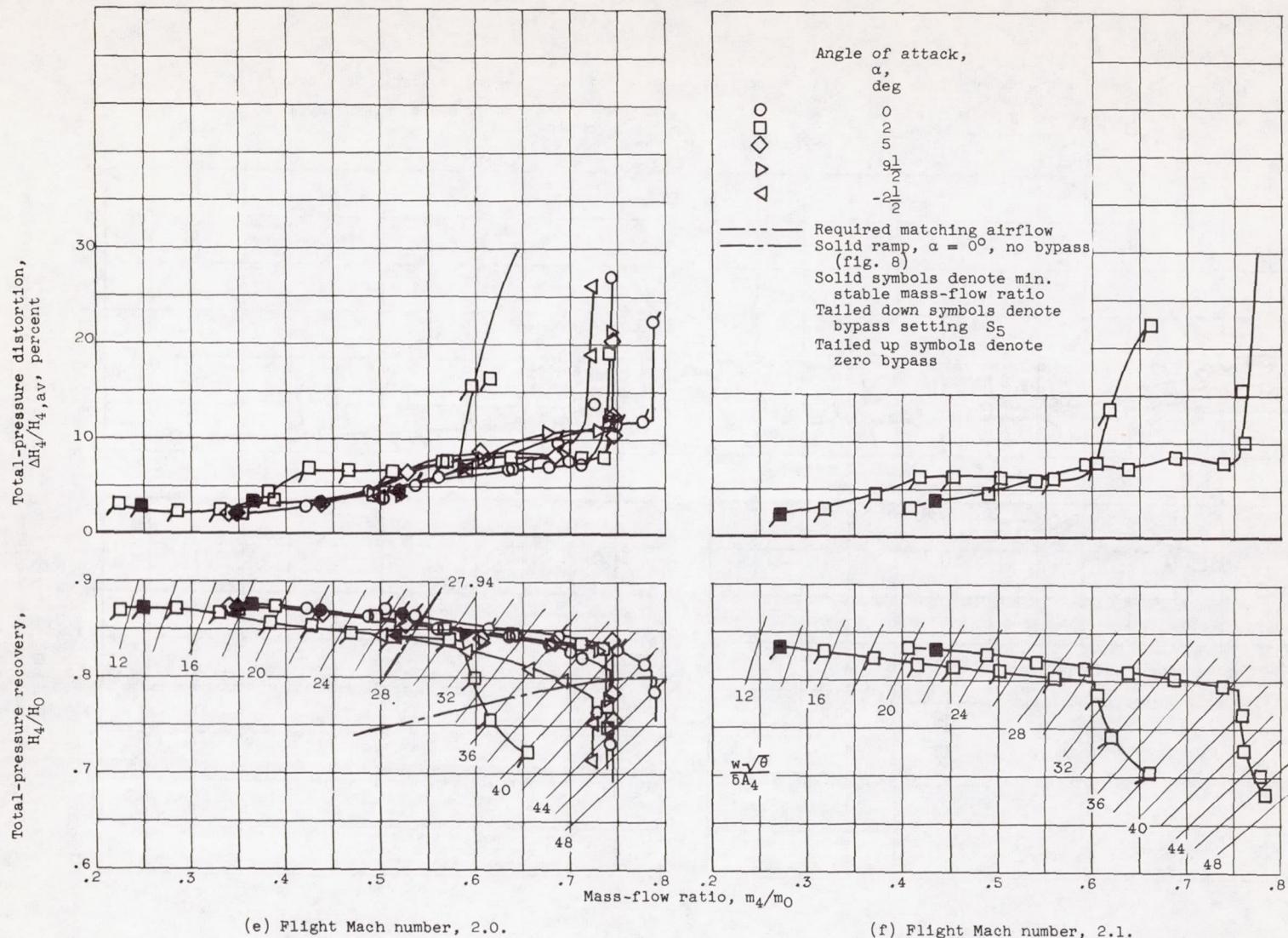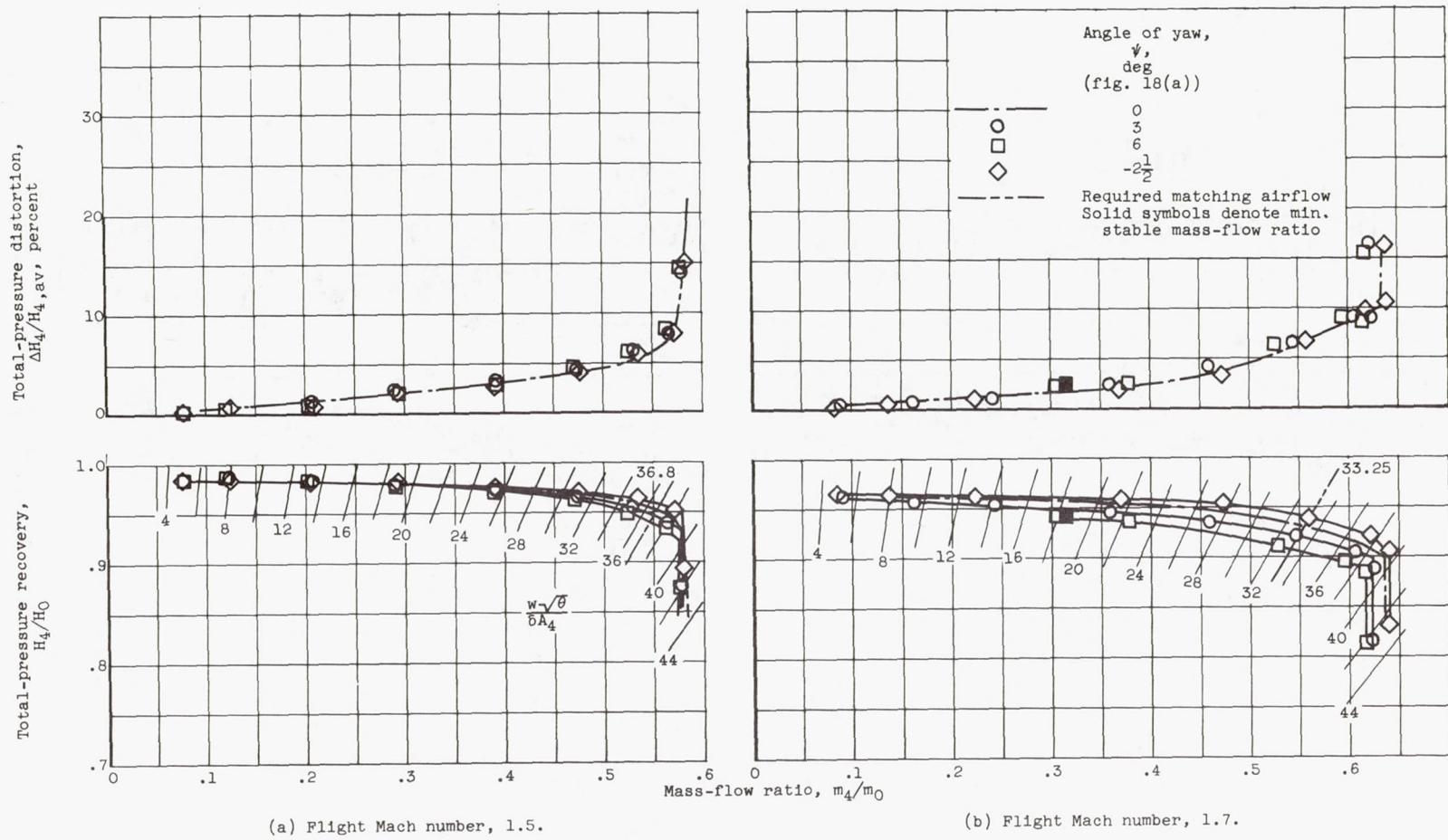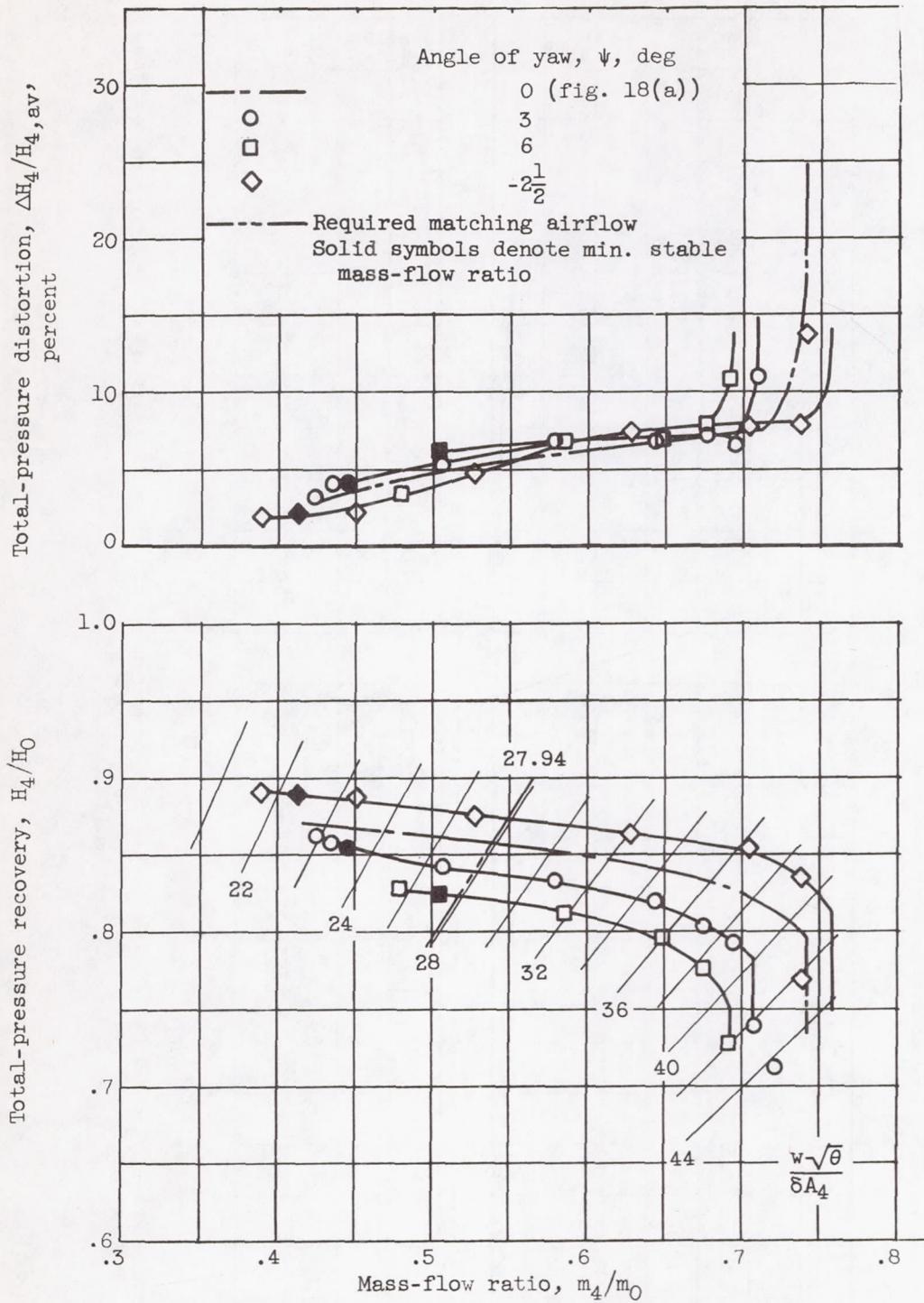(e) Flight Mach number, 2.0.

(f) Flight Mach number, 2.1.

Figure 19. - Concluded. Effect of flight Mach number and angle of attack on inlet performance with A_8V perforated ramp and bypass setting S_1 (unless noted).

(a) Flight Mach number, 1.5.

(b) Flight Mach number, 1.7.

Figure 20. - Effect of angle of yaw on inlet performance with A_8V ramp and bypass setting S_1.

(c) Flight Mach number, 2.0.

Figure 20. - Concluded. Effect of angle of yaw on inlet performance with A_8V ramp and bypass setting S_1.
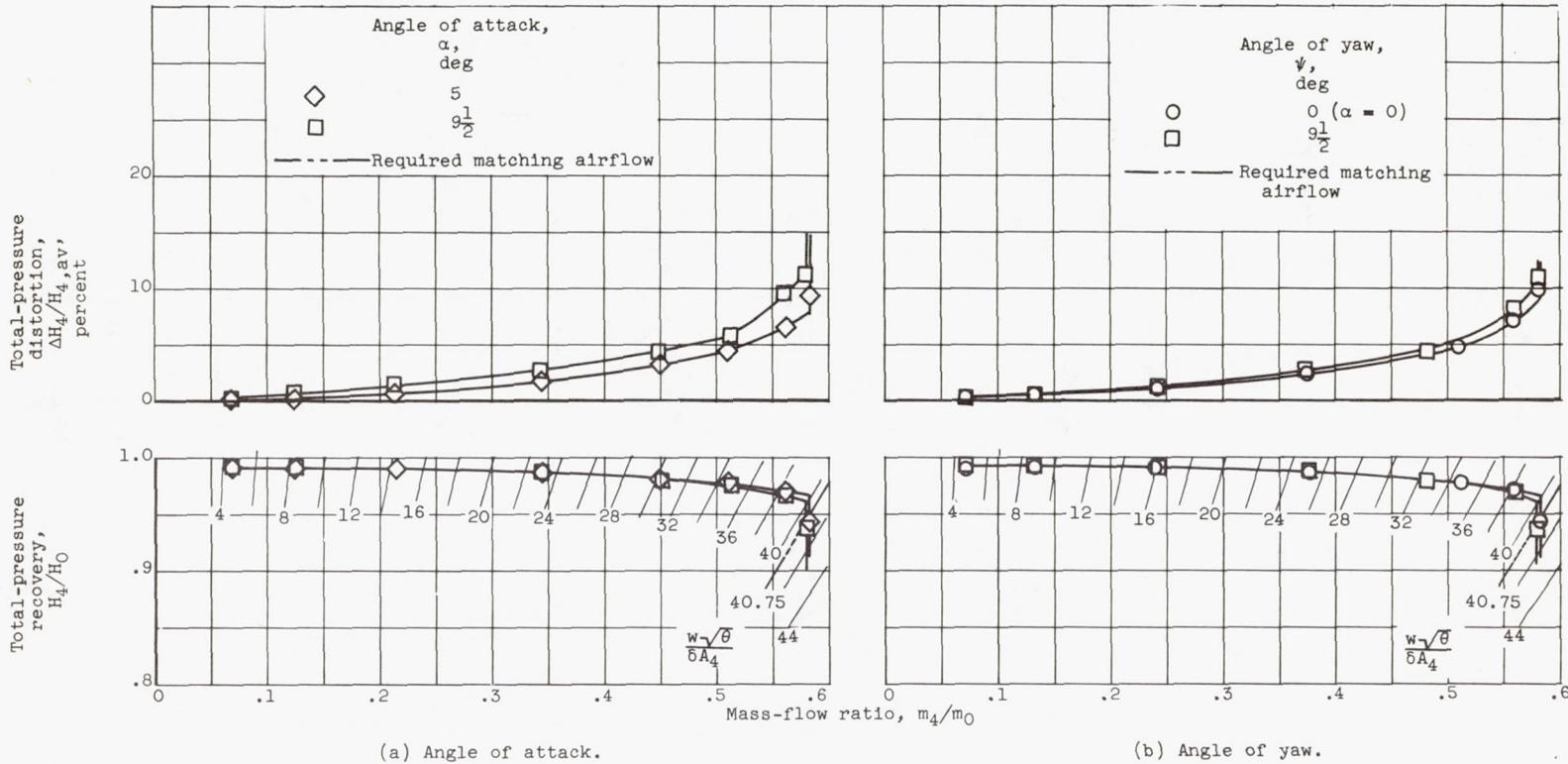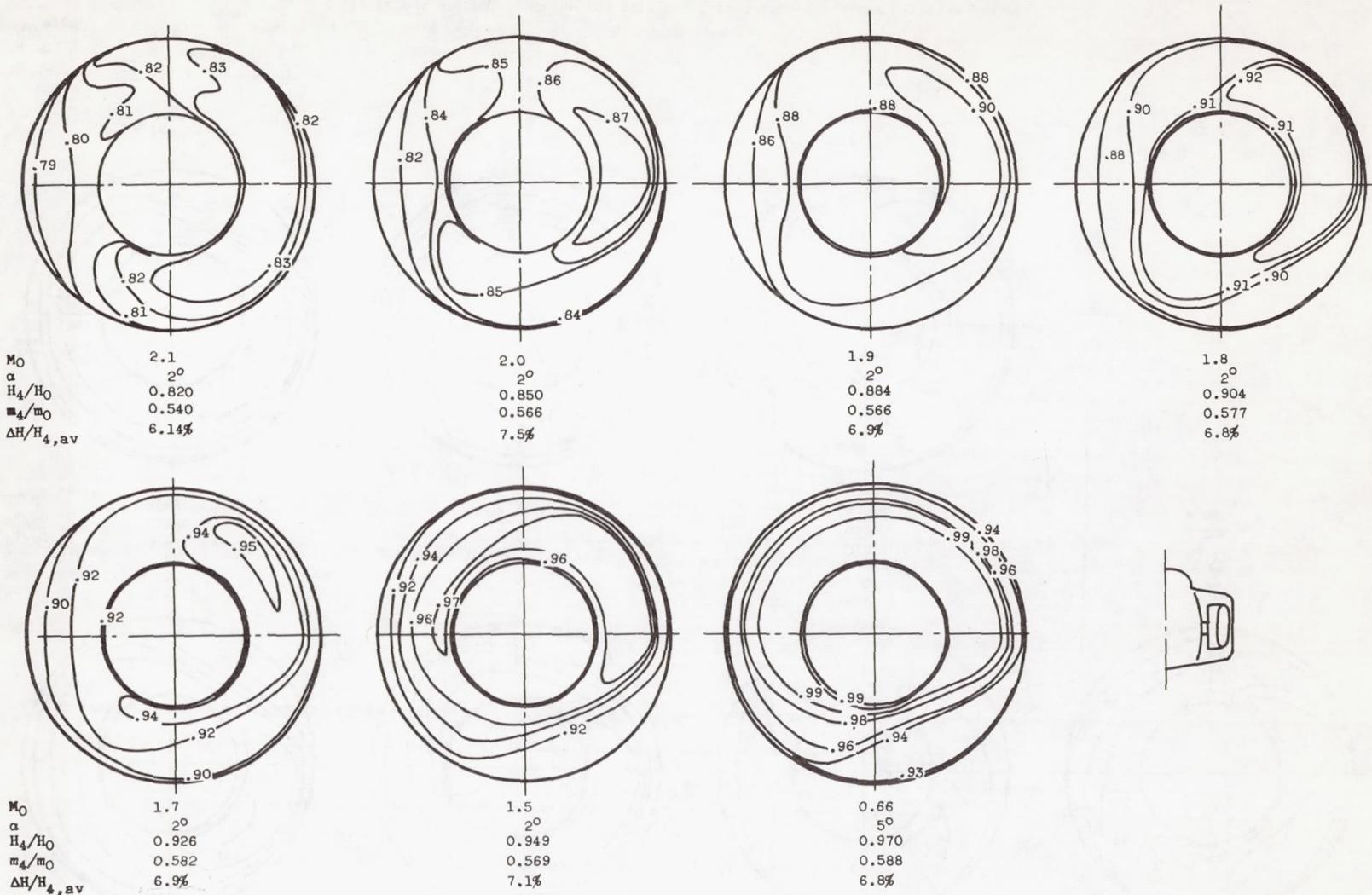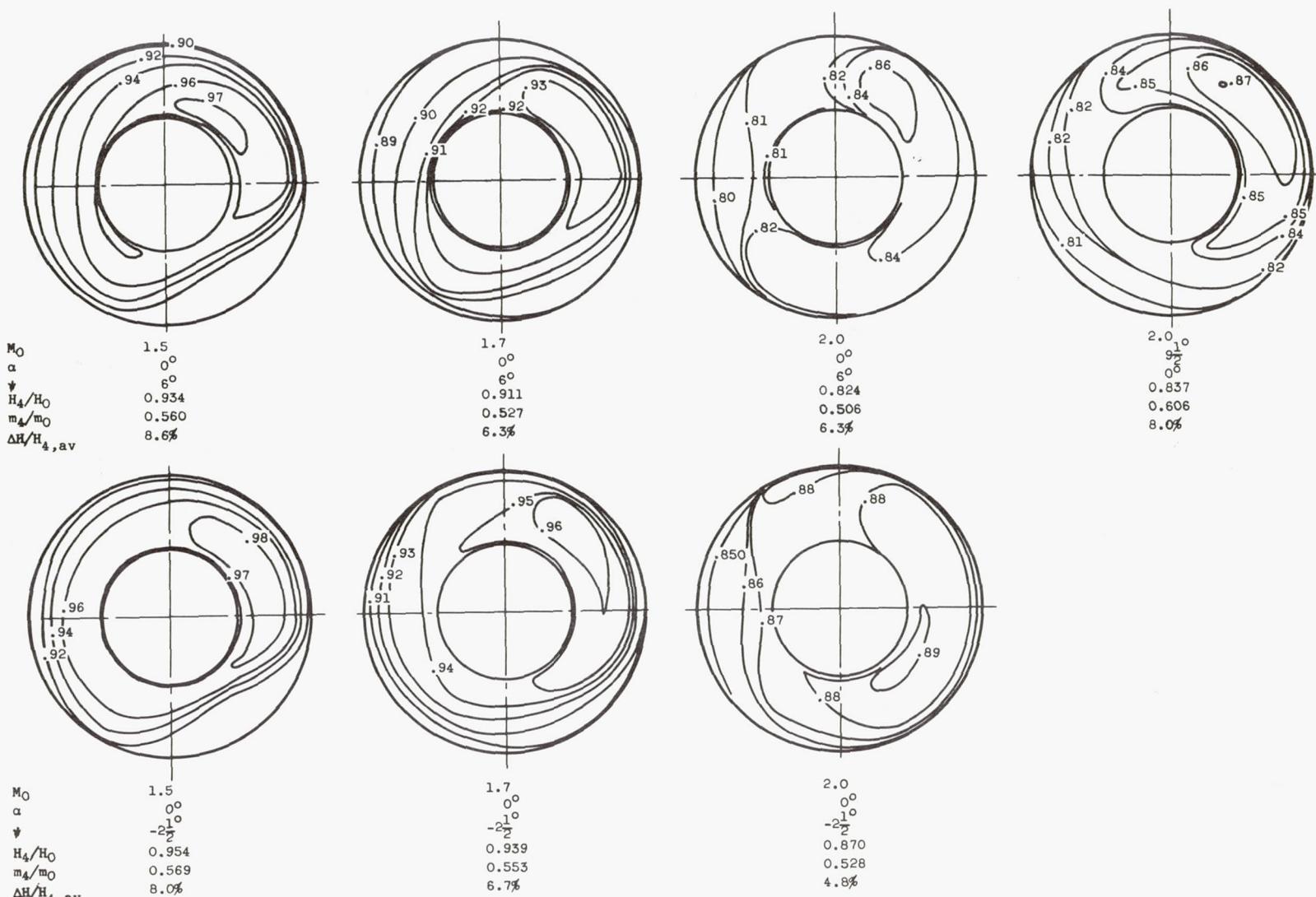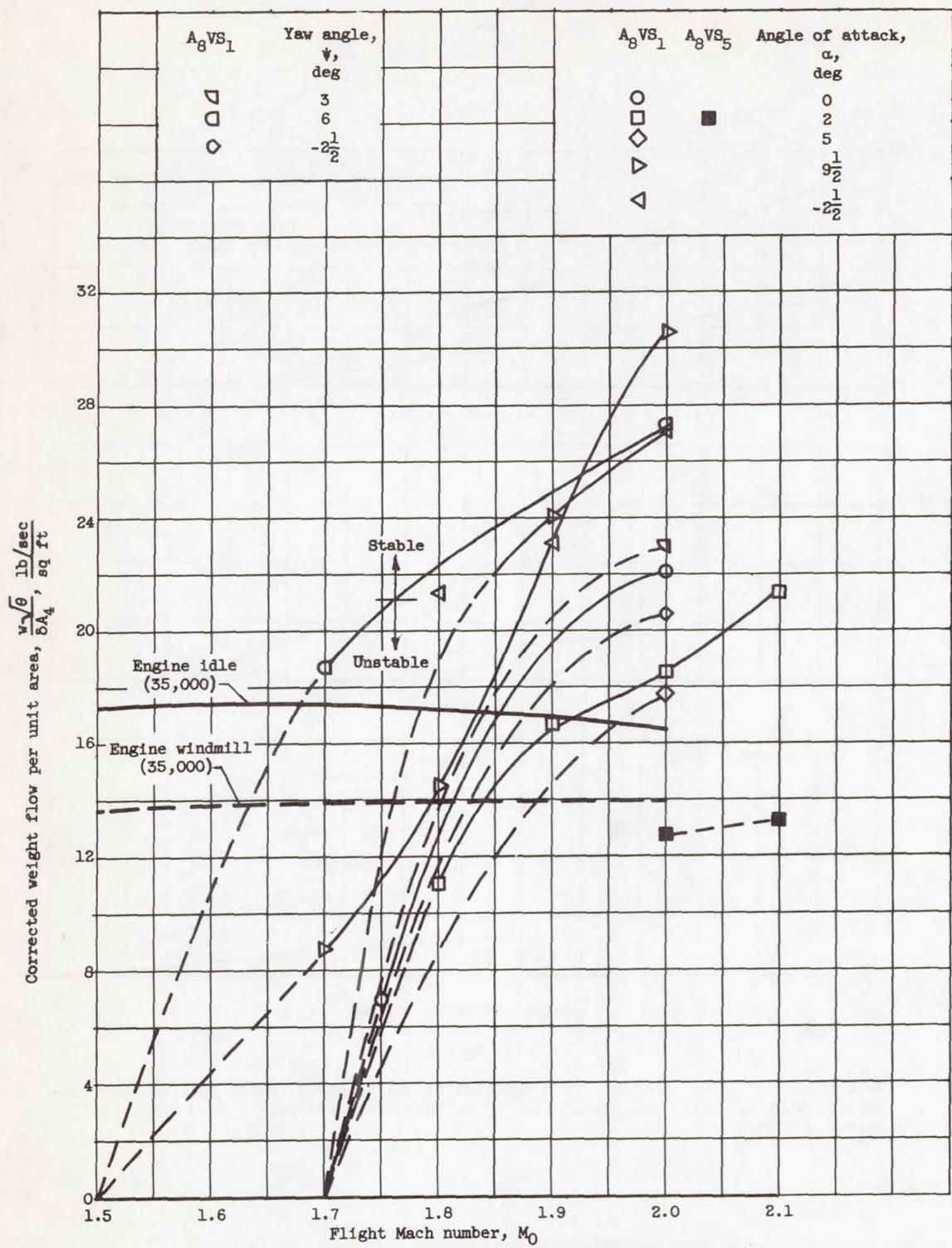
(a) Angle of attack.

(b) Angle of yaw.

Figure 21. - Effect of angles of attack or yaw at flight Mach number of 0.66 on inlet performance with A_8V ramp and bypass setting S_1.

M_0	2.1	2.0	1.9	1.8
α	2°	2°	2°	2°
H_4/H_0	0.820	0.850	0.884	0.904
m_4/m_0	0.540	0.566	0.566	0.577
$\Delta H/H_{4,av}$	6.14%	7.5%	6.9%	6.8%

M_0	1.7	1.5	0.66
α	2°	2°	5°
H_4/H_0	0.926	0.949	0.970
m_4/m_0	0.582	0.569	0.588
$\Delta H/H_{4,av}$	6.9%	7.1%	6.8%

(a) Effect of flight Mach number. Yaw angle, 0°.

Figure 22. - Total-pressure contours at station 4 near engine matching conditions. Configuration A_8VS_1.

M_O	1.5	1.7	2.0	2.0
α	0°	0°	0°	$9\frac{1}{2}^o$
ψ	6°	6°	6°	0°
H_4/H_O	0.934	0.911	0.824	0.837
m_4/m_O	0.560	0.527	0.506	0.606
$\Delta H/H_{4,av}$	8.6%	6.3%	6.3%	8.0%

M_O	1.5	1.7	2.0
α	0°	0°	0°
ψ	$-2\frac{1}{2}^o$	$-2\frac{1}{2}^o$	$-2\frac{1}{2}^o$
H_4/H_O	0.954	0.939	0.870
m_4/m_O	0.569	0.553	0.528
$\Delta H/H_{4,av}$	8.0%	6.7%	4.8%

(b) Effect of angles of yaw and attack. (Inlet is leeward for positive angles.)

Figure 22. - Concluded. Total-pressure contours at station 4 near engine matching conditions. Configuration A_8VS_1.

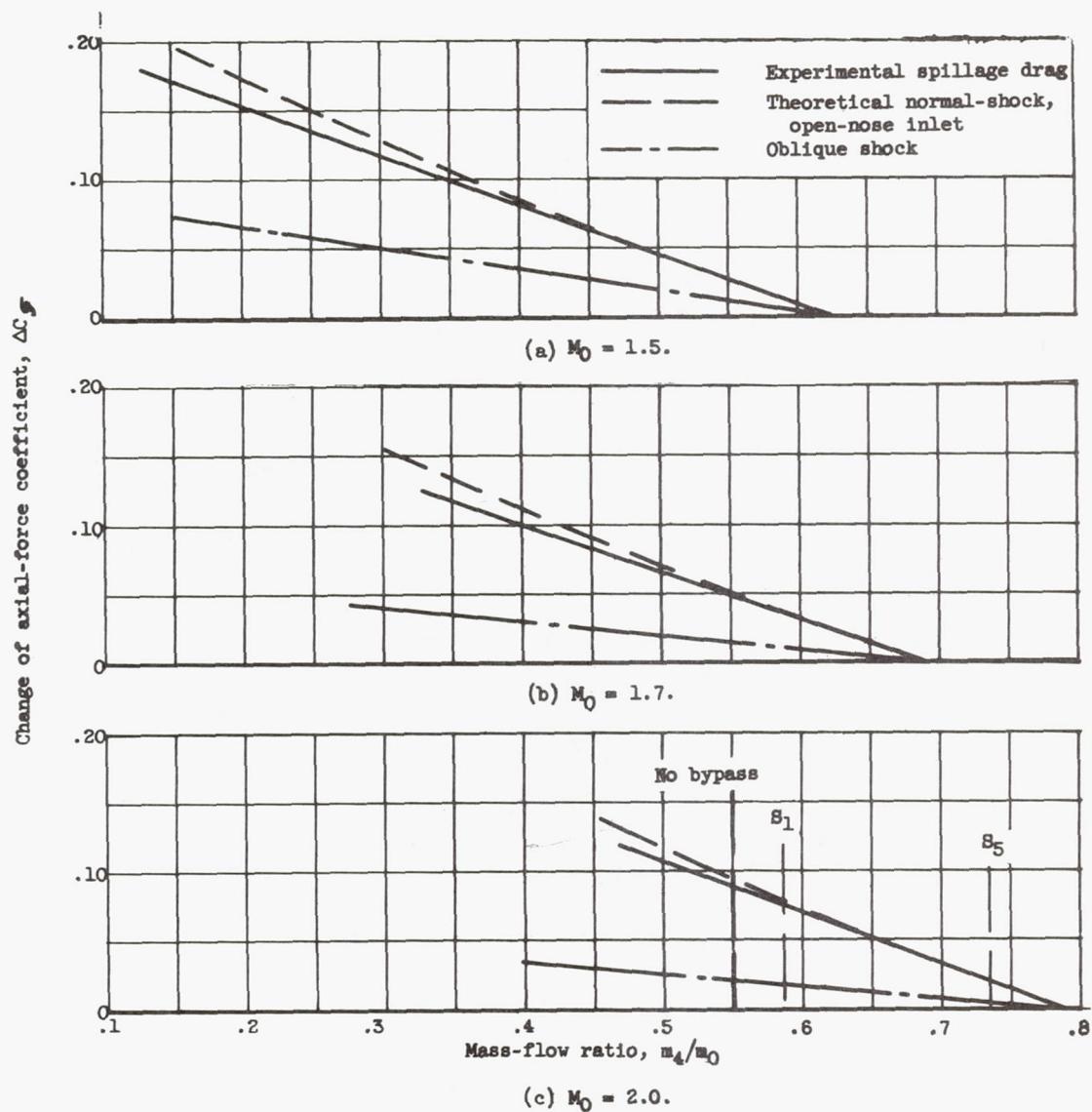Figure 23. - Summary of stability limits; A_8V ramp.

Figure 24. - Variation of axial-force coefficient due to normal-shock spillage and comparison with additive drag for normal- or oblique-shock spillage. Zero angles of attack and yaw.
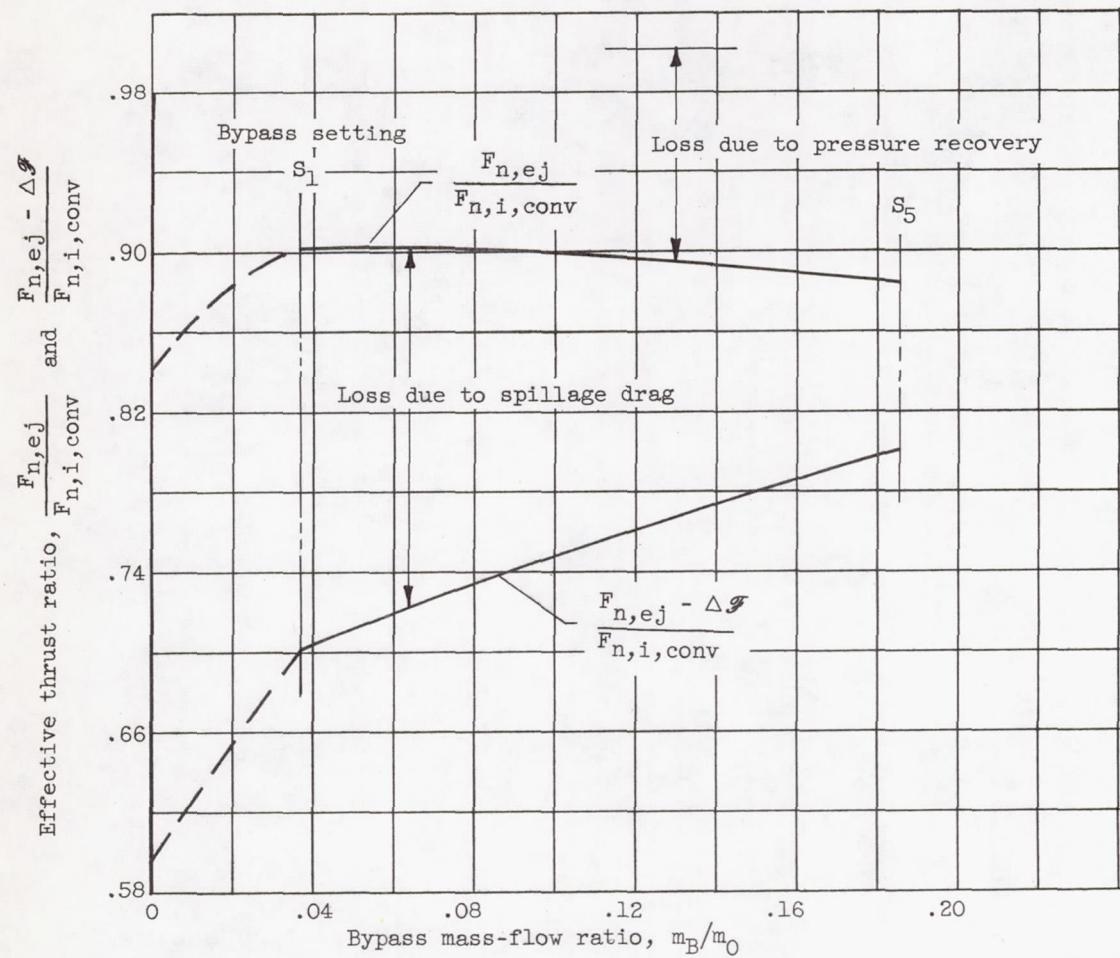
Figure 25. - Effect of bypass and ejector on effective thrust ratio at engine matching conditions. Flight Mach number, 2.0.